POLITECNICO DI TORINO

Laurea Magistrale in Ingegneria Matematica

Politecnico
di Torino

Tesi di Laurea Magistrale

A CONFORMING/NON-CONFORMING APPROACH TO THE COMPUTATION OF FLOW IN DISCRETE FRACTURE NETWORKS

Relatore
Prof. Stefano BERRONE

Candidato
Stefano CHIOLA

Correlatore
Dott. Fabio VICINI

Novembre 2023

Abstract

Two numerical methods for the computation of flow in Discrete Fracture Networks (DFNs) are discussed, modeling the distribution of the pressure of a fluid in an impermeable fractured medium. The first method is based on a mesh which conforms to the intersection between fractures (traces), using the Virtual Element Method (VEM), while the second follows an optimization approach, with distinct meshes on each fracture, not conforming to the traces. The behaviors of the two approaches are investigated and compared on two numerical test cases. Finally, a joint approach is proposed with the intent of potentially mitigating the drawbacks and exploiting the advantages of the two methods.

Ad Alessia,
ai miei Nonni,
i miei Genitori
e mio Fratello

Table of Contents

List of Tables VI

List of Figures VII

1 Introduction 1
- 1.1 Notation . . . 1
- 1.2 Problem setting . . . 2
- 1.3 Weak formulation . . . 2
- 1.4 Numerical techniques . . . 5

2 Virtual Element Method 7
- 2.1 Virtual element space . . . 7
- 2.2 Approximated forms and discrete problem . . . 9

3 Conforming VEM approach 11
- 3.1 Conforming mesh . . . 11
- 3.2 Discretization with elements of order 1 . . . 11
- 3.3 Numerical Results . . . 13

4 Non-conforming optimization approach 17
- 4.1 Optimal control formulation . . . 17
- 4.2 Discrete formulation . . . 19
- 4.3 Numerical results . . . 22

5 Joint approach 27
- 5.1 Optimal control formulation . . . 27
- 5.2 Discrete formulation . . . 29

6 Conclusions 31

Bibliography 33

List of Tables

4.1 Convergence slopes of the average flux mismatch and hydraulic head jump norms on traces, for Frac3 and Frac36. 23

List of Figures

3.1 Frac3 (top) and Frac36 (bottom) DFNs and corresponding conforming approach numerical solutions, in color. 14
3.2 Convergence to the exact solution for Frac3 in L^2 and H^1 norms, for decreasing δ, for the three fractures and average convergence orders. . . 15
3.3 Condition number of A for Frac3 (points), for varying δ, and the corresponding trend line, with slope -2.28. 15

4.1 Convergence to the exact solution for Frac3 in L^2 and H^1 norms, for decreasing δ, for the three fractures and average convergence orders. . . 23
4.2 Condition number of $\mathcal{A}$ for Frac3 (points), for varying δ_H, and the corresponding slope lines. The results are shown for values of $\frac{\delta_U}{\delta_H} = .5, 1, 2, 3, 4$. The average slope is -2.15 24
4.3 From the top, condition number of $\mathcal{A}$, trace mesh size, hydraulic head jump and flux mismatch norms, plotted against varying values of the ratio $\frac{\delta_U}{\delta_H}$, for Frac3 with $\delta_H = 1.8 \cdot 10^{-2}$ on the left and Frac36 with $\delta_H = 2.8 \cdot 10^{-2}$ on the right. 25
4.4 Average flux mismatch (top) and hydraulic head jump (bottom) for Frac3, for varying δ_H, and the corresponding slope lines. The results are shown for values of $\frac{\delta_U}{\delta_H} = .5, 2, 4$. 26
4.5 Average flux mismatch (top) and hydraulic head jump (bottom) for Frac36, for varying δ_H, and the corresponding slope lines. The results are shown for values of $\frac{\delta_U}{\delta_H} = .5, 2, 4$. 26

Chapter 1

Introduction

The study of fluid flow in fracture networks is relevant in many practical applications, such as modeling of groundwater resources, dispersion of contaminants, oil and gas deposits management. Fractures in an impermeable medium can be modeled as intersecting plane polygons, on which the fluid flow is assumed to present a Darcian linear dependence on the hydraulic head gradient. Additional continuity conditions are required at intersections between fractures (traces). In this work, two ways to enforce such conditions are considered, resulting in two different approaches. The first approach relies on a discretization of the fractures with a mesh which conforms to the traces, using the Virtual Element Method to handle the different polygonal shapes of the elements for which some of the edges are part of the traces. The second method follows an optimization approach, with distinct meshes on each fracture, not conforming to the traces, in which an appropriate functional is minimized, constrained by the field equations on each fracture. In this Chapter, the continuous model of fluid flow is presented. In Chapter 2, the Virtual Element Method is introduced for a generic elliptic problem and is then applied to the discrete fracture network problem in Chapter 3. In Chapter 4, the optimization-based approach is presented. Finally, in Chapter 5 a new joint approach is formulated, informed by the numerical experiments performed with the first two methods.

1.1 Notation

Throughout this work, the standard L^2 scalar product over a domain $\mathcal{D}$ or a line Γ will be denoted, respectively, as

$$(v, w)_{\mathcal{D}}, \qquad (v, w)_{\Gamma},$$

for every $v, w \in L^2(\mathcal{D})$ or $v, w \in L^2(\Gamma)$. Similarly, the notation

$$(\nabla v, \nabla w)_{\mathcal{D}} := \int_{\mathcal{D}} \nabla v \cdot \nabla w$$

is used for functions $v, w \in H^1(\mathcal{D})$.

1.2 Problem setting

Consider a network of N fractures in three-dimensional (3D) space, represented by as many intersecting plane polygons $F_i \subset \mathbb{R}^3$, $i \in \mathfrak{I}$. The problem of subsurface fracture flow can be stated on the whole fracture network $\Omega = \bigcup_{i\in\mathfrak{I}} F_i$ as

$$\nabla \cdot (\boldsymbol{K}\nabla H) = Q \quad \text{in } \Omega, \tag{1.1}$$

$$H_{|\Gamma_D} = H_D \quad \text{on } \Gamma_D, \tag{1.2}$$

$$\frac{\partial H}{\partial \nu_{\Gamma_N}} = G_N \quad \text{on } \Gamma_N, \tag{1.3}$$

where $\partial\Omega = \Gamma_D \cup \Gamma_N$ and $\Gamma_D \neq \emptyset$, H is the hydraulic head, $\boldsymbol{K}$ is the transmissivity tensor and $\frac{\partial H}{\partial \nu_{\Gamma_N}} = \boldsymbol{n}_{\Gamma_N}^T \boldsymbol{K}\nabla H$ is the outward co-normal derivative of the hydraulic head, with $\boldsymbol{n}_{\Gamma_N}$ the unit vector outward normal to the boundary Γ_N. Throughout the scope of this work, the transmissivity tensor is supposed to be isotropic, of the form $\boldsymbol{K} = \hat{k}\boldsymbol{I}$, such that there exist two constants $k_* > 0$ and $k^* > 0$ such that

$$k_* \leq \hat{k} \leq k^*.$$

Note that the derivatives in 1.1 and 1.3 are meant along a reference system tangential to the appropriate fracture. Furthermore, for $i \in \mathfrak{I}$, define $\Gamma_{iD} = \Gamma_D \cap \partial F_i$ and $\Gamma_{iN} = \Gamma_N \cap \partial F_i$. Let $H_i := H_{|_{F_i}}$, $Q_i := Q_{|_{F_i}}$ and $\boldsymbol{K}_i := \boldsymbol{K}_{|_{F_i}}$ denote the restrictions of the hydraulic head, the forcing term and the trasmissivity tensor to the fracture F_i. Let $G_{iN} = G_{N|_{\Gamma_{iN}}}$, $G_{iD} = G_{D|_{\Gamma_{iD}}}$. Let $\mathcal{S}$ be the set of all intersections, called traces, $S_m = F_i \cap F_j$ between two fractures, with S_m of non vanishing measure, with index $m \in \mathfrak{M}$. For each trace S_m, let $I_{S_m} = \{i, j\}$ be the set of the indices of the two fractures such that $S_m = F_i \cap F_j$. Define also $\mathcal{S}_i = \{S_m \in \mathcal{S} : S_m \subset F_i\}$. Define the jump across the trace S_m of the co-normal derivative of the hydraulic head in fracture F_i as

$$\left[\!\left[\frac{\partial H_i}{\partial \nu^i_{S_m}} \right]\!\right]_{S_m} := \left. \frac{\partial H_i}{\partial \nu^i_{S_m}} \right|_{F_i^+} - \left. \frac{\partial H_i}{\partial \nu^i_{S_m}} \right|_{F_i^-},$$

with $\boldsymbol{n}^i_{S_m}$ being a unit vector normal to the trace S_m in the plane of F_i and the symbols '+' and '−' referring, respectively, to the side of S_m towards which $\boldsymbol{n}^i_{S_m}$ is pointing and the opposite one. This quantity is independent on the choice of $\boldsymbol{n}^i_{S_m}$. The continuity of hydraulic pressure and the conservation of fluxes between intersecting fractures is guaranteed by the conditions

$$H_{i|_{S_m}} = H_{j|_{S_m}} \quad \text{on } S_m \tag{1.4}$$

$$\left[\!\left[\frac{\partial H_i}{\partial \nu^i_{S_m}} \right]\!\right]_{S_m} + \left[\!\left[\frac{\partial H_j}{\partial \nu^j_{S_m}} \right]\!\right]_{S_m} = 0 \quad \text{on } S_m \tag{1.5}$$

on each trace S_m.

1.3 Weak formulation

Define for each fracture the spaces

$$V_i = H^1_0(F_i) = \{v \in H^1(F_i) : v_{|\Gamma_{iD}} = 0\}$$

and

$$V_i^D = H_D^1(F_i) = \{v \in H^1(F_i) : v_{|\Gamma_{iD}} = H_{iD}\},$$

then the restriction $H_i = H_{|F_i}$ of the hydraulic head to the fracture F_i belongs to the space V_i^D, and the hydraulic head H on the whole Ω belongs to the space

$$V^D = H_D^1(\Omega) = \left\{ v \in \prod_{i\in\mathfrak{I}} V_i^D : \left(v_{|F_i}\right)_{|S_m} = \left(v_{|F_j}\right)_{|S_m}, i,j \in I_{S_m}, \forall m \in \mathfrak{M} \right\}.$$

Similarly, define

$$V = H_0^1(\Omega) = \left\{ v \in \prod_{i\in\mathfrak{I}} V_i : \left(v_{|F_i}\right)_{|S_m} = \left(v_{|F_j}\right)_{|S_m}, i,j \in I_{S_m}, \forall m \in \mathfrak{M} \right\}.$$

For the spaces V_i and V_i^D, define the norms

$$\begin{aligned} \|v\|_{V_i} &:= \|\nabla v\|_{(L^2(F_i))^2} \qquad \text{if } \Gamma_{iD} \neq \emptyset, \\ \|v\|_{V_i} &:= \left[\|\nabla v\|^2_{(L^2(F_i))^2} + \|v\|^2_{L^2(F_i)}\right]^{\frac{1}{2}} \quad \text{if } \Gamma_{iD} = \emptyset, \end{aligned}$$

$$\|v\|_{V_i^D} := \left[\|\nabla v\|^2_{(L^2(F_i))^2} + \|v\|^2_{L^2(F_i)}\right]^{\frac{1}{2}}.$$

For the spaces V and V^D, consider the norms

$$\|v\|_V := \left[\sum_{i\in\mathfrak{I}} \|v\|^2_{V_i}\right]^{\frac{1}{2}}, \qquad \|v\|_{V^D} := \left[\sum_{i\in\mathfrak{I}} \|v\|^2_{V_i^D}\right]^{\frac{1}{2}}.$$

Starting from the governing equation 1.1, the problem of flow on fractures can be posed in weak form as follows. Let $v \in V$ be a test function on the domain. Multiplying equation 1.1 by v and integrating on Ω, one has

$$\sum_{i\in\mathfrak{I}} \int_{F_i} \nabla \cdot (\boldsymbol{K}_i \nabla H_i)\, v_{|F_i}\, \mathrm{d}F_i = \sum_{i\in\mathfrak{I}} \int_{F_i} Q_i v_{|F_i}\, \mathrm{d}F_i.$$

To apply Green's Theorem to the left hand side, introduce the set of subfractures f_l, $l \in \mathfrak{L}$ consisting of the open polygons obtained by cutting each fracture F_i along the directions of the traces $S \in \mathcal{S}_i$. One has then

$$\begin{aligned} \sum_{i\in\mathfrak{I}} \int_{F_i} \nabla \cdot (\boldsymbol{K}_i \nabla H_i)\, v_{|F_i}\, \mathrm{d}F_i &= \sum_{l\in\mathfrak{L}} \int_{f_l} \nabla \cdot \left(\boldsymbol{K}_{f_l} \nabla H_{|f_l}\right) v_{|f_l}\, \mathrm{d}f_l = \\ &= \sum_{i\in\mathfrak{I}} \int_{F_i} \boldsymbol{K}_i \nabla H_i \cdot \nabla v_{|F_i}\, \mathrm{d}F_i - \sum_{l\in\mathfrak{L}} \int_{\partial f_l} \left(\boldsymbol{K}_{f_l} \nabla H_{|f_l} \cdot \boldsymbol{n}_{\partial f_l}\right) v_{|f_l}\, \mathrm{d}\Gamma. \end{aligned} \tag{1.6}$$

Each subfracture boundary can be decomposed as

$$\partial f_l = \left[\partial f_l \cap \left(\bigcup_{m\in\mathfrak{M}} S_m\right)\right] \cup \left[\partial f_l \cap \partial\Omega\right] \cup \partial f_l^{\text{int}} = \partial f_l^{\text{t}} \cup \partial f_l^{\text{b}} \cup \partial f_l^{\text{int}}, \tag{1.7}$$

where 't' and 'b' stand respectively for 'traces' and 'boundary', and $\partial f_l^{\text{int}}$ denotes the portion of the subfracture boundary that is neither part of traces nor of fracture boundaries. The boundary term is then, denoting by $\frac{\partial}{\partial \nu}$ the directional derivative along the appropriate outward unit vector $\boldsymbol{n}$ co-normal to the curve along which each integral is performed,

$$
\begin{aligned}
-\sum_{l\in\mathfrak{L}}\int_{\partial f_l}\left(\boldsymbol{K}_{f_l}\nabla H_{|_{f_l}}\cdot\boldsymbol{n}_{\partial f_l}\right)v_{|_{f_l}}\,\mathrm{d}\Gamma &= -\sum_{l\in\mathfrak{L}}\int_{\partial f_l}\frac{\partial H_{|_{f_l}}}{\partial\nu}v_{|_{\partial f_l}}\,\mathrm{d}\Gamma = \\
&= -\sum_{l\in\mathfrak{L}}\left[\int_{\partial f_l^{\mathrm{t}}}\frac{\partial H_{|_{f_l}}}{\partial\nu}v_{|_{\partial f_l^{\mathrm{t}}}}\,\mathrm{d}\Gamma+\int_{\partial f_l^{\mathrm{b}}}\frac{\partial H_{|_{f_l}}}{\partial\nu}v_{|_{\partial f_l^{\mathrm{b}}}}\,\mathrm{d}\Gamma+\int_{\partial f_l^{\mathrm{int}}}\frac{\partial H_{|_{f_l}}}{\partial\nu}v_{|_{\partial f_l^{\mathrm{int}}}}\,\mathrm{d}\Gamma\right] \\
&= -\sum_{i\in\mathfrak{I}}\sum_{S\in\mathcal{S}_i}\int_S\left[\!\!\left[\frac{\partial H_i}{\partial\nu_S^i}\right]\!\!\right](v_{|_{F_i}})_{|_S}\,\mathrm{d}\Gamma-\sum_{i\in\mathfrak{I}}\int_{\partial F_i}\frac{\partial H_i}{\partial\nu}v_{|_{\partial F_i}}\,\mathrm{d}\Gamma, \qquad (1.8)
\end{aligned}
$$

where the sum on subfractures has been substituted with one on fractures and $\boldsymbol{n}_S^i$ is a unique unit vector co-normal to the trace S in the plane of fracture F_i. The sum over $l\in\mathfrak{L}$ of the integrals over $\partial f_l^{\text{int}}$ vanishes. Indeed, calling $\Gamma_i^{\text{int}}:=\bigcup_{f_l\subset F_i}\partial f_l^{\text{int}}$, one has

$$
\sum_{l\in\mathfrak{L}}\int_{\partial f_l^{\mathrm{int}}}\frac{\partial H_{|_{f_l}}}{\partial\nu}v_{|_{\partial f_l^{\mathrm{int}}}}\,\mathrm{d}\Gamma=\sum_{i\in\mathfrak{I}}\int_{\Gamma_i^{\mathrm{int}}}\left[\!\!\left[\frac{\partial H_i}{\partial\nu^i_{\Gamma_i^{\mathrm{int}}}}\right]\!\!\right](v_{|_{F_i}})_{|_{\Gamma_i^{\mathrm{int}}}}\,\mathrm{d}\Gamma=0.
$$

The first term of 1.8, regarding the traces, can be rewritten as

$$
\sum_{i\in\mathfrak{I}}\sum_{S\in\mathcal{S}_i}\int_S\left[\!\!\left[\frac{\partial H_i}{\partial\nu_S^i}\right]\!\!\right](v_{|_{F_i}})_{|_S}\,\mathrm{d}\Gamma=\sum_{S\in\mathcal{S}}\int_S\left\{\left[\!\!\left[\frac{\partial H_i}{\partial\nu_S^i}\right]\!\!\right]+\left[\!\!\left[\frac{\partial H_j}{\partial\nu_S^j}\right]\!\!\right]\right\}v_{|_S}\,\mathrm{d}\Gamma. \qquad (1.9)
$$

This is only possible thanks to the choice of space V, which guarantees that for each $S\in\mathcal{S}$, $(v_{|_{F_i}})_{|_S}=(v_{|_{F_j}})_{|_S}=:v_{|_S}$, $\{i,j\}=I_S$. Therefore conditions 1.5 on flux conservation on traces are enforced in the weak form imposing that the term 1.9 be zero $\forall v\in V$. The second boundary term of 1.8, related to the boundary conditions, gives

$$
\begin{aligned}
\sum_{i\in\mathfrak{I}}\int_{\partial F_i}\frac{\partial H_i}{\partial\nu}v_{|_{\partial F_i}}\,\mathrm{d}\Gamma &= \sum_{i\in\mathfrak{I}}\int_{\Gamma_{iN}}\frac{\partial H_i}{\partial\nu}v_{|_{\Gamma_{iN}}}\,\mathrm{d}\Gamma+\sum_{i\in\mathfrak{I}}\int_{\Gamma_{iD}}\frac{\partial H_i}{\partial\nu}v_{|_{\Gamma_{iD}}}\,\mathrm{d}\Gamma \\
&= \sum_{i\in\mathfrak{I}}\int_{\Gamma_{iN}}\frac{\partial H_i}{\partial\nu}v_{|_{\Gamma_{iN}}}\,\mathrm{d}\Gamma \\
&= \sum_{i\in\mathfrak{I}}\int_{\Gamma_iN}G_{iN}v_{|_{\Gamma_iN}}\,\mathrm{d}\Gamma. \qquad (1.10)
\end{aligned}
$$

The resulting weak form of the problem is then

Find $H\in V^D$ s.t.

$$
\sum_{i\in\mathfrak{I}}\int_{F_i}\boldsymbol{K}_i\nabla H_i\cdot\nabla v_{|_{F_i}}\,\mathrm{d}\Omega=\sum_{i\in\mathfrak{I}}\int_{F_i}Q_iv_{|_{F_i}}\,\mathrm{d}\Omega+\sum_{i\in\mathfrak{I}}\int_{\Gamma_{iN}}G_{iN}v_{|_{\Gamma_{iN}}}\,\mathrm{d}\Gamma,\quad\forall v\in V \qquad (1.11)
$$

which resembles the one for a 2D domain. The problem in this form is well posed, thanks to the Lax-Milgram Theorem. Indeed the bilinear form

$$
a^{\Omega}(w,v):=\sum_{i\in\mathfrak{I}}\int_{F_i}\boldsymbol{K}_i\nabla w_{|_{F_i}}\cdot\nabla v_{|_{F_i}}\,\mathrm{d}\Omega,\quad\forall v,w\in V
$$

is continuous and coercive on V and the functional

$$F^{\Omega}(v) := \sum_{i\in\mathfrak{I}} \int_{F_i} Q_i v_{|_{F_i}} \, \mathrm{d}\Omega + \sum_{i\in\mathfrak{I}} \int_{\Gamma_{iN}} G_{iN} v_{|_{\Gamma_{iN}}} \, \mathrm{d}\Gamma, \quad \forall v \in V \tag{1.12}$$

is continuous on V, requiring $Q_i \in L^2(F_i)$ and $G_{iN} \in L^2(\Gamma_{iN})$, $i \in \mathfrak{I}$.

1.4 Numerical techniques

For the discretization of problem 1.1-1.5, two different methods to impose the conditions on the traces will be considered. The first [4] consists in conforming the meshes of the two intersecting domains so that the degrees of freedom associated with the nodes and the edges of the triangulation on the trace are shared between the two domains. Even if the meshes on the domains are triangular, this results in more generic polygonal elements where the triangles need to be cut to achieve conformity. This suggests the use of the Virtual Element Method, which can handle such shapes. This approach results in a discretization of the form 1.11. On the other hand, the second approach [7, 8] consists in the construction of an appropriate functional to be minimized in order to reach an approximate satisfaction of the conditions on the traces. The field equations on each domain act as a constraint in the minimization. This approach does not require any conformity of the domains' meshes and is well suited for a parallel implementation [10].

Chapter 2

Virtual Element Method

The Virtual Element Method (VEM) can be considered as an extension of the finite element method to elements of more general polygonal and polyhedral shape. The VEM still uses functional spaces containing polynomials of degree k to recover convergence results, however the basis functions are not in general polynomial and never computed explicitly, not even in an approximate way. They are used only trough the values of their degrees of freedom. This feature is what gives the name "virtual" to the elements. In the following, a variation [1] of the standard VEM formulation [2] is presented for the elliptic 2D problem

$$-\nabla \cdot (\boldsymbol{K} \nabla H) = Q \quad \text{in } \mathcal{D} \subset \mathbb{R}^2$$

with homogeneous Dirichlet boundary conditions on $\partial\mathcal{D}$. In weak form this yields

$$\textbf{Find } H \in H_0^1(\mathcal{D}) \text{ s.t. } a^{\mathcal{D}}(H, v) = F^{\mathcal{D}}(v) \quad \forall v \in H_0^1(\mathcal{D}), \tag{2.1}$$

with

$$a^{\mathcal{D}}(w, v) := (\boldsymbol{K} \nabla w, \nabla v)_{\mathcal{D}}, \quad F^{\mathcal{D}}(v) := (Q, v)_{\mathcal{D}}, \quad w, v \in H_0^1(\mathcal{D}). \tag{2.2}$$

With assumptions similar to those given in Chapter 1, problem 2.1 is well posed.

2.1 Virtual element space

Consider a partition $\mathcal{T}_\delta$ of the domain $\mathcal{D} \subset \mathbb{R}^2$, $\mathcal{D} = \bigcup_{E \in \mathcal{T}_\delta} E$, where each $E \in \mathcal{T}_\delta$ is a simple, star-shaped polygon, such that the length of its edges decreases at most with order 1 with δ [1, 2]. For each polygon E, the number of vertices is denoted by N^E, while the polygon's area, centroid and diameter are noted respectively as $|E|$, $\boldsymbol{x}_E$ and d_E. For each polygon E, consider the following local space, defined for values of $k = 1, 2, 3, \ldots$

$$V_k(E) = \Big\{ v \in H^1(E) \,:\, v_{|_{e_i}} \in \mathbb{P}_k(e_i), i = 1, \ldots, N^E, \quad v_{|_{\partial E}} \in C^0(\partial E), \quad \Delta v \in \mathbb{P}_k(E), \\ \big(p, \Pi_{k,E}^{\nabla}(v) - v\big)_E = 0 \quad \forall p \in \mathbb{P}_k(E) \setminus \mathbb{P}_{k-2}(E) \Big\}, \tag{2.3}$$

where $\mathbb{P}_k(E) \setminus \mathbb{P}_{k-2}(E)$ is the set of polynomials exactly of order k and $k-1$ and by convention $\mathbb{P}_{-1}(E) = \{0\}$. The operator $\Pi^{\nabla}_{k,E} : H^1(E) \to \mathbb{P}_k(E)$ is defined such that for every $v \in H^1(E)$

$$\left(\nabla p, \nabla(\Pi^{\nabla}_{k,E} v - v)\right)_E = 0 \quad \forall p \in \mathbb{P}_k(E), \tag{2.4}$$

$$\left(1, \Pi^{\nabla}_{k,E} v - v\right)_{\partial E} = 0 \quad \text{if } k = 1, \tag{2.5}$$

$$\left(1, \Pi^{\nabla}_{k,E} v - v\right)_E = 0 \quad \text{if } k > 1. \tag{2.6}$$

One has $\mathbb{P}_k(E) \subseteq V_k(E)$, since a polynomial of degree k on E satisfies all the conditions in definition 2.3. In particular the last condition in 2.3 holds because

$$\Pi^{\nabla}_{k,E}(q) = q, \quad \forall q \in \mathbb{P}_k(E).$$

Indeed, from 2.4, $\nabla(\Pi^{\nabla}_{k,E}(q) - q) \in (\mathbb{P}_{k-1}(E))^2$ is zero, therefore $\Pi^{\nabla}_{k,E}(q) - q \in \mathbb{P}_0(E)$, and from 2.5 or 2.6 one has $\Pi^{\nabla}_{k,E}(q) - q = 0$.

Consider the following set of degrees of freedom (dofs) for $V_k(E)$

- $\mathcal{V}^{E,k}$: the values of v at the vertices of the polygon;
- $\mathcal{E}^{E,k}$: if $k > 1$, the values of v at the $k-1$ internal nodes of the Gauss-Lobatto quadrature rule on each edge;
- $\mathcal{P}^{E,k}$: if $k > 1$, the moments $\frac{1}{|E|}(v, m_{\boldsymbol{\alpha}})_E$ of order up to $k-2$ of v, where $m_{\boldsymbol{\alpha}} = \left(\frac{\boldsymbol{x}-\boldsymbol{x}_E}{d_E}\right)^{\boldsymbol{\alpha}}$, with $\boldsymbol{\alpha} = (\alpha_1, \alpha_2)$, $|\boldsymbol{\alpha}| = \alpha_1 + \alpha_2$, $|\boldsymbol{\alpha}| = 1, \ldots, k-2$, and for a generic vector $\boldsymbol{x}$, $\boldsymbol{x}^{\boldsymbol{\alpha}} = x_1^{\alpha_1} x_2^{\alpha_2}$.

Let $\mathrm{dof}_i^E(v_\delta)$ denote the degrees of freedom of $v_\delta \in V_k(E)$, numbered from 1 to N_E^{dof} and define the functions $\varphi_i \in V_k(E)$ so that

$$\mathrm{dof}_i^E(\varphi_j) = \delta_{ij}, \qquad i, j = 1, \ldots, N_E^{\mathrm{dof}}.$$

Proposition. *$\mathcal{V}^{E,k}$, $\mathcal{E}^{E,k}$, $\mathcal{P}^{E,k}$ are a unisolvent set of dofs for $V_k(E)$.*

Proof. Assigning the dofs $\mathcal{V}^{E,k}$ and $\mathcal{E}^{E,k}$ uniquely determines a polynomial in $\mathbb{P}_k(e)$ on each edge e of E, therefore uniquely defining a function $v \in V_k(E)$ on the boundary ∂E. Moreover, if all the dofs $\mathcal{V}^{E,k}$ and $\mathcal{E}^{E,k}$ are zero, then $v = 0$ on ∂E. On the other hand, the assignment of the dofs $\mathcal{P}^{E,k}$ uniquely determines the L^2-orthogonal projection $P^E_{k-2} v \in \mathbb{P}_{k-2}(E)$ of $v \in V_k(E)$, and $P^E_{k-2} v = 0$ in E if all the dofs $\mathcal{P}^{E,k}$ are zero. Furthermore, also the L^2-orthogonal projection $P^E_k v \in \mathbb{P}_k(E)$ is zero. Indeed, [3] shows how $\Pi^{\nabla}_{k,E}(v)$ can be computed solely through the values of the dofs of v listed above. In particular if the dofs are all zero, then $\Pi^{\nabla}_{k,E}(v) = 0$. Thanks to the definition 2.3, it then holds that

$$(p, v) = (p, \Pi^{\nabla}_{k,E}(v)) = 0, \quad \forall p \in \mathbb{P}_k(E) \setminus \mathbb{P}_{k-2}(E)$$

and therefore

$$(m_{\boldsymbol{\alpha}}, v) = 0, \quad k - 1 \leq |\boldsymbol{\alpha}| \leq k,$$

which, together with $P^E_{k-2} v = 0$, implies $P^E_k v = 0$.

If $v \in V_k(E)$ is such that $v = 0$ on ∂E and $P_k^E v = 0$ in E, then $v = 0$ in E. Indeed, analogously to the proof given in [2], for every $q \in \mathbb{P}_k(E)$ solve the auxiliary Dirichlet problem

$$\textbf{Find } w \in H_0^1(E) \text{ s.t.} \qquad a^E(w, z) = (q, z)_E, \quad \forall z \in H_0^1(E) \tag{2.7}$$

and denote the solution as $w = -\Delta_{0,E}^{-1}(q)$. The map $R : \mathbb{P}_k(E) \to \mathbb{P}_k(E)$ defined as

$$Rq := P_k^E(-\Delta_{0,E}^{-1}(q)) \equiv P_k^E w$$

is an isomorphism [2] and in particular

$$Rq = 0 \iff q = 0.$$

Since $v = 0$ on ∂E,

$$P_k^E v = P_k^E(-\Delta_{0,E}^{-1}(-\Delta v)) = R(-\Delta v).$$

Then $P_k^E v = 0 \implies R(-\Delta v) = 0 \implies -\Delta v = 0$, which, together with $v = 0$ on ∂E, implies $v = 0$ in E. □

The number of dofs N_E^{dof} corresponds to the dimension of the space $V_k(E)$

$$\dim V_k(E) = N_E^{\text{dof}} = N^E + (k-1)N^E + \frac{k(k-1)}{2} = kN^E + \frac{k(k-1)}{2}$$

and the functions $\varphi_i \in V_k(E)$ constitute the canonical basis of $V_k(E)$. Then each function $v \in V_k(E)$ can be expressed as

$$v = \sum_{i=1}^{N_E^{\text{dof}}} \text{dof}_i^E(v)\varphi_i.$$

If all polygons in the mesh are equipped with the virtual element space and dofs, considering homogeneous Dirichlet boundary conditions, the resulting global space is

$$V_k^{\mathcal{D}} = \{v \in H_0^1(\mathcal{D}) \,:\, v_{|_E} \in V_k(E) \quad \forall E \in \mathcal{T}_\delta\}, \tag{2.8}$$

equipped with the global dofs

- $\mathcal{V}^k$: the values of v at the internal mesh vertices;
- $\mathcal{E}^k$: if $k > 1$, the values of v at the $k-1$ internal nodes of the Gauss-Lobatto quadrature rule on each internal edge of the mesh;
- $\mathcal{P}^k$: if $k > 1$, the moments $\frac{1}{|E|}(v, m_{\boldsymbol{\alpha}})_E$ of order up to $k-2$ of v on each polygon E.

2.2 Approximated forms and discrete problem

Since the expression of the basis functions of the space $V_k(E)$ is not known, the forms 2.2 cannot be computed. The exact forms $a^{\mathcal{D}}(\cdot,\cdot)$ and $F^{\mathcal{D}}(\cdot)$ are substituted with the approximated ones $a_\delta^{\mathcal{D}}(\cdot,\cdot)$ and $F_\delta^{\mathcal{D}}(\cdot)$. Let $a^E(\cdot,\cdot)$ and $F^E(\cdot)$ be the restrictions of $a^{\mathcal{D}}$ and $F^{\mathcal{D}}$ to an element E and $a_\delta^E(\cdot,\cdot)$ and $F_\delta^E(\cdot)$ the restrictions of the approximated

forms. In the following, assume that $\boldsymbol{K} = \hat{k}\boldsymbol{I}$ is constant on the domain $\mathcal{D}$. In the remainder of this Chapter, denote as Π^∇ the local projection $\Pi^\nabla_{k,E}$, for simplicity of notation. Note that by expressing a generic function $v \in V_k(E)$ as

$$v = \Pi^\nabla v + (\mathrm{I} - \Pi^\nabla)v,$$

one can rewrite $a^E(w, v)$, for every $w, v \in V_k(E)$, as

$$\begin{aligned}(\boldsymbol{K}\nabla w, \nabla v)_E =& (\boldsymbol{K}\nabla\Pi^\nabla w, \nabla\Pi^\nabla v)_E + (\boldsymbol{K}\nabla(\mathrm{I} - \Pi^\nabla)w, \nabla(\mathrm{I} - \Pi^\nabla)v)_E \\ &+ (\boldsymbol{K}\nabla\Pi^\nabla w, \nabla(\mathrm{I} - \Pi^\nabla)v)_E + (\boldsymbol{K}\nabla(\mathrm{I} - \Pi^\nabla)w, \nabla\Pi^\nabla v)_E,\end{aligned}$$

where the last two terms are zero, thanks to condition 2.4 and $\boldsymbol{K}$ being constant, giving

$$a^E(w, v) = (\boldsymbol{K}\nabla\Pi^\nabla w, \nabla\Pi^\nabla v)_E + (\boldsymbol{K}\nabla(\mathrm{I} - \Pi^\nabla)w, \nabla(\mathrm{I} - \Pi^\nabla)v)_E. \tag{2.9}$$

In the current implementation, the form 2.9 is approximated as

$$a^E_\delta(w, v) := \hat{k}(P^E_{k-1}(\nabla w), P^E_{k-1}(\nabla v))_E + \hat{k}\sum_{r=1}^{N^{\mathrm{dof}}_E} \mathrm{dof}^E_r((\mathrm{I} - \Pi^\nabla)w)\,\mathrm{dof}^E_r((\mathrm{I} - \Pi^\nabla)v), \tag{2.10}$$

following [1]. The functions $P^E_{k-1}(\nabla v)$ and $\Pi^\nabla v$ can be computed through the dofs of v, for any $v \in V_k(E)$ [1, 3]. The functional F^E is substituted by the approximation [1]

$$F^E_\delta(v) := (Q, P^E_{k-1}v)_E. \tag{2.11}$$

Define the discrete problem

$$\textbf{Find } h \in V^\mathcal{D}_k \text{ s.t. } a^\mathcal{D}_\delta(h, v) = F^\mathcal{D}_\delta(v) \quad \forall v \in V^\mathcal{D}_k, \tag{2.12}$$

with the choices 2.10 and 2.11 for the forms a_δ and F_δ. It has been proved in [1] that problem 2.12 is well posed and that the following error estimates hold, for H and Q sufficiently regular:

$$\|H - h\|_{H^1(\mathcal{D})} \leq C\delta^k \left(\|H\|_{H^{k+1}(\mathcal{D})} + |Q|_{k,\mathcal{D}}\right), \tag{2.13}$$

$$\|H - h\|_{L^2(\mathcal{D})} \leq C\delta^{k+1} \left(\|H\|_{H^{k+1}(\mathcal{D})} + |Q|_{k,\mathcal{D}}\right), \tag{2.14}$$

with $|Q|_{k,\mathcal{D}}$ being the k-th order Sobolev seminorm of Q on $\mathcal{D}$.

Chapter 3

Conforming VEM approach

One possibility to enforce the conditions 1.4 and 1.5 in a discrete setting is to conform the meshes of the two intersecting fractures to each other on the traces. In this way the global degrees of freedom (dofs) associated to the mesh nodes on the traces are shared by the two fractures generating it. Conformity can be achieved meshing the fracture polygons independently and then cutting the cells which intersect with a trace. Note that this operation changes the shape of the cells touching the trace. Therefore, even if the independent meshing process on the fractures returns a mesh with cells all of the same shape, for instance triangular, the final mesh will contain polygons with a different number of vertices. Furthermore, these polygons may present hanging nodes, that is vertices between collinear edges. These properties suggest the use of virtual elements. For the first order case, virtual and finite elements can be easily integrated to produce a discretization with both element types, where the virtual elements are used only for the polygons with more than three vertices, while finite elements are used for the triangles.

3.1 Conforming mesh

The mesh for the domain is constructed following the approach of [4], in which, for each fracture, a triangular mesh is generated first, independently of the other fractures. A local conformity is then achieved on each fracture cutting the elements that intersect with the traces. The new edges introduced by the cuts are then enriched with the nodes corresponding to the vertices of the polygons obtained through the cutting process on the other fracture sharing the trace. This yields a conforming mesh $\mathcal{T}_\delta$ on the domain Ω.

3.2 Discretization with elements of order 1

The set of polygons $\mathcal{T}_\delta$ of the conforming mesh described above is partitioned into $\mathcal{T}_\delta^{\text{VEM}} \cup \mathcal{T}_\delta^{\text{FEM}} = \mathcal{T}_\delta$. A polygon is assigned to $\mathcal{T}_\delta^{\text{VEM}}$ if it has more than three vertices and to $\mathcal{T}_\delta^{\text{FEM}}$ otherwise. Virtual element and finite element discretizations are used on the cells in $\mathcal{T}_\delta^{\text{VEM}}$ and $\mathcal{T}_\delta^{\text{FEM}}$, resulting in the local spaces $V_k^{\text{VEM}}(E) = V_k(E)$, for $E \in \mathcal{T}_\delta^{\text{VEM}}$, as defined in 2.3, and $V_k^{\text{FEM}}(E) = \mathbb{P}_k(E)$, for $E \in \mathcal{T}_\delta^{\text{FEM}}$. For the FEM spaces choose the standard Lagrangian local dofs. On an internal edge e dividing a VEM cell from a FEM cell of the same order $k = 1$, the dofs on e for both cells are the same; in fact the only dofs on e are the values of the function at the extremities. In this

way, the dofs on the boundary of the elements are the same for the two kinds of spaces, allowing for a straightforward gluing of the elements, giving the global discrete spaces

$$\begin{aligned} V_\delta^{D,1} = \big\{ v \in V^D : v_{|E_{\text{VEM}}} \in V_1^{\text{VEM}}(E_{\text{VEM}}) \quad \forall E_{\text{VEM}} \in \mathcal{T}_\delta^{\text{VEM}}, \\ v_{|E_{\text{FEM}}} \in V_1^{\text{FEM}}(E_{\text{FEM}}) \quad \forall E_{\text{FEM}} \in \mathcal{T}_\delta^{\text{FEM}} \big\}, \\ V_\delta^{1} = \big\{ v \in V : v_{|E_{\text{VEM}}} \in V_1^{\text{VEM}}(E_{\text{VEM}}) \quad \forall E_{\text{VEM}} \in \mathcal{T}_\delta^{\text{VEM}}, \\ v_{|E_{\text{FEM}}} \in V_1^{\text{FEM}}(E_{\text{FEM}}) \quad \forall E_{\text{FEM}} \in \mathcal{T}_\delta^{\text{FEM}} \big\}, \end{aligned}$$

of dimensions

$$N^D := \dim V_\delta^{D,1}, \qquad N := \dim V_\delta^1.$$

Since $V_\delta^1 \subset V$, for any $v_\delta \in V_\delta^1$ it is still true that $\left(v_{\delta|_{F_i}}\right)_{|_S} = \left(v_{\delta|_{F_j}}\right)_{|_S}$, $\{i,j\} = I_S$, on each trace $S \in \mathcal{S}$, and analogously for $V_\delta^{D,1}$. Note that the nodes of the mesh lying on the traces are shared by the elements in both of the intersecting fractures, therefore the associated dof is also shared and the corresponding basis function is non-zero on both fractures. A unisolvent set of global dofs for $v_\delta \in V_\delta^{D,1}$, resulting from the matching of the local dofs on the element boundaries, is

- $\mathcal{V}^1$: the values of v_δ at the mesh vertices V.

The same set of functionals, but without those related to Dirichlet boundaries, gives a set of dofs for V_δ^1. Consider a numbering of the global dofs of $V_\delta^{D,1}$ from $1, \dots, N^D$ such that the first N are the dofs of V_δ^1 and denote with $\text{dof}_i(v_\delta)$ the i-th degree of freedom of a function $v_\delta \in V_\delta^{D,1}$. Define the canonical basis functions $\varphi_i \in V_\delta^{D,1}$, for $i = 1, \dots, N^D$ such that

$$\text{dof}_i(\varphi_j) = \delta_{ij}, \quad j = 1, \dots, N^D. \tag{3.1}$$

Define the quantity

$$h = \sum_{i=1}^{N^D} h_i \varphi_i = h^0 + h^D, \tag{3.2}$$

representing the discrete counterpart of the solution H, expressed through appropriate coefficients h_i in the canonical basis, where $h^0 \in V_\delta^1$ and $h^D \in V_\delta^{D,1}$ is the lifting of the Dirichlet boundary conditions imposed on Γ_D. Consider the setting of the weak form 1.11 in the subspaces $V_\delta^{D,k} \subset V^D$, $V_\delta^k \subset V$, substituting the exact forms with the approximated ones

$$\begin{aligned} a_\delta^\Omega(w,v) := \sum_{E \in \mathcal{T}_\delta^{\text{VEM}}} \hat{k}_E \Bigg\{ & (P_0^E(\nabla w), P_0^E(\nabla v))_E + \\ & \sum_{r=1}^{N_E^{\text{dof}}} \text{dof}_r^E((\mathrm{I} - \Pi_{1,E}^\nabla)w)\, \text{dof}_r^E((\mathrm{I} - \Pi_{1,E}^\nabla)v) \Bigg\} + \sum_{E \in \mathcal{T}_\delta^{\text{FEM}}} \hat{k}_E (\nabla w, \nabla v)_E, \\ F_\delta^\Omega(v) := \sum_{E \in \mathcal{T}_\delta^{\text{VEM}}} (Q, P_0^E v)_E + \sum_{E \in \mathcal{T}_\delta^{\text{FEM}}} (Q, v)_E, & \end{aligned}$$

defined $\forall w \in V_\delta^{D,k}$, $\forall v \in V_\delta^k$ following the choices presented in Chapter 2 for the VEM elements, with $k = 1$, where homogeneous Neumann boundary conditions on Γ_N were assumed, together with the choice $\boldsymbol{K}_i = \hat{k}_i \boldsymbol{I}$, with $\hat{k}_i > 0$ constant, $i \in \mathfrak{I}$. For an element E, the notation $\hat{k}_E := \hat{k}_i$ was used, where i is the index of the fracture containing E. The resulting discrete problem

$$\textbf{Find } h \in V_\delta^{D,k} \text{ s.t.} \quad a_\delta^\Omega(h, v) = F_\delta^\Omega(v), \quad \forall v \in V_\delta^k$$

is equivalent to the linear system

$$Ah^0 = f - A^D h^D, \tag{3.3}$$

where, with an overload of notation for h^0 and h^D,

$$\begin{aligned}
&A \in \mathbb{R}^{N \times N}, && A_{ij} := a_\delta^\Omega(\varphi_j, \varphi_i), && 1 \le i, j \le N, \\
&A^D \in \mathbb{R}^{N \times N^D - N}, && A^D_{ij} := a_\delta^\Omega(\varphi_{N+j}, \varphi_i), && 1 \le i \le N, \quad 1 \le j \le N^D - N, \\
&f \in \mathbb{R}^N, && f_i := F_\delta^\Omega(\varphi_i), && 1 \le i \le N, \\
&h^0 \in \mathbb{R}^N, && h^0_i := h_i, && 1 \le i \le N, \\
&h^D \in \mathbb{R}^{N^D - N}, && h^D_j := h_{N+j}, && 1 \le j \le N^D - N.
\end{aligned}$$

3.3 Numerical Results

The approach described in this Chapter is tested on two DFN cases with 3 and 36 fractures, called Frac3 and Frac36 respectively, depicted in Figure 3.1. In Frac3, specific non-homogeneous Dirichlet boundary conditions are set on all boundaries and a non-zero forcing term is used, for which the exact solution is known [5]. In Frac36, 0 and 1 constant Dirichlet boundary conditions are set each on a particular edge of two distant fractures, while homogeneous Neumann boundary conditions are set for the rest of the boundary and no forcing term is present, mimicking a case in which a fluid flows across a set of fractures without losses.

Convergence results are presented in Figure 4.1 for Frac3. The discretization parameter δ^2 controls the areas of the triangles of the fracture meshes, which are then cut to achieve conformity. The L^2 error shows an average convergence order of 1.91, while the H^1 error converges with order 0.90 with respect to the parameter δ, in agreement with the VEM and FEM estimates.

Figure 3.3 shows the dependence of the condition number of A on δ_H for the test Frac3. The condition number diverges approximately as δ^{-2}.

It is important to note that the conforming process can lead to meshes with elements characterized by very high aspect ratio or very small angles, which can significantly degrade the quality of the solution, especially for higher orders of approximation [4]. This can happen for example when two traces are very close to each other or they intersect forming a very slight angle.

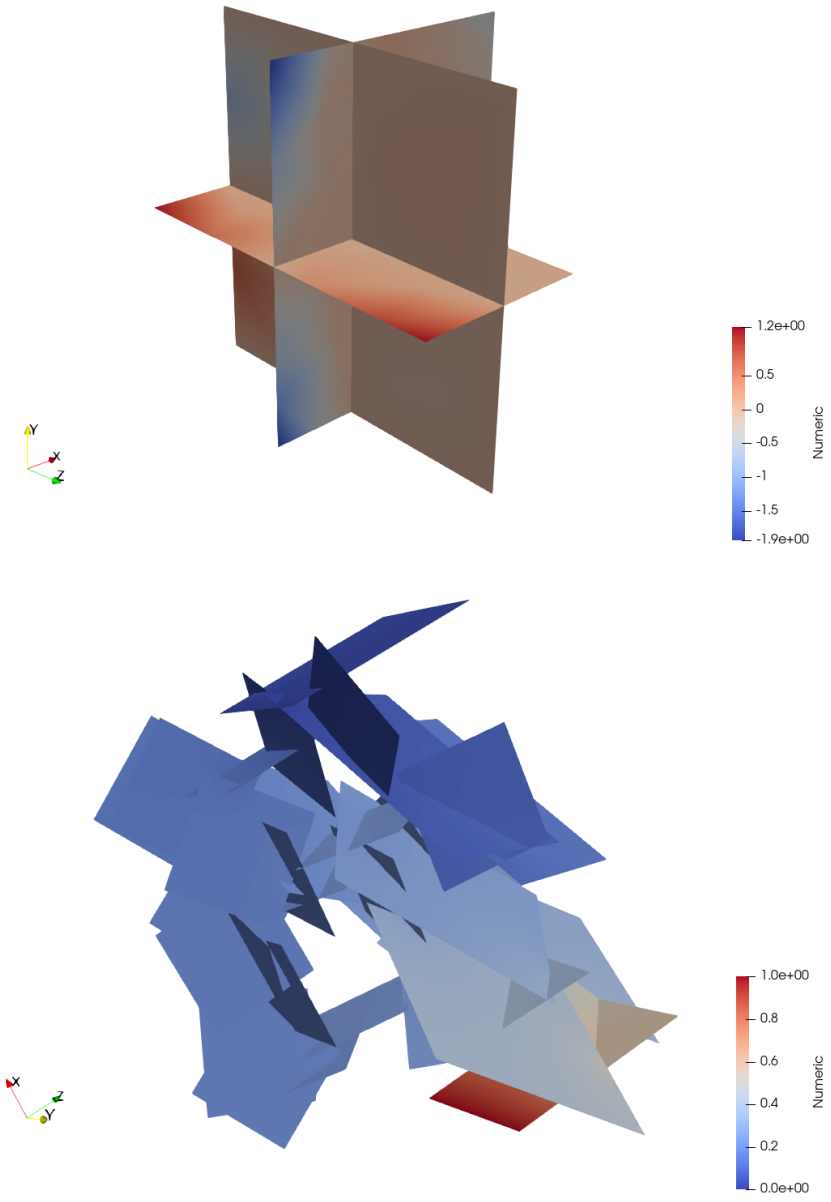

Figure 3.1. Frac3 (top) and Frac36 (bottom) DFNs and corresponding conforming approach numerical solutions, in color.

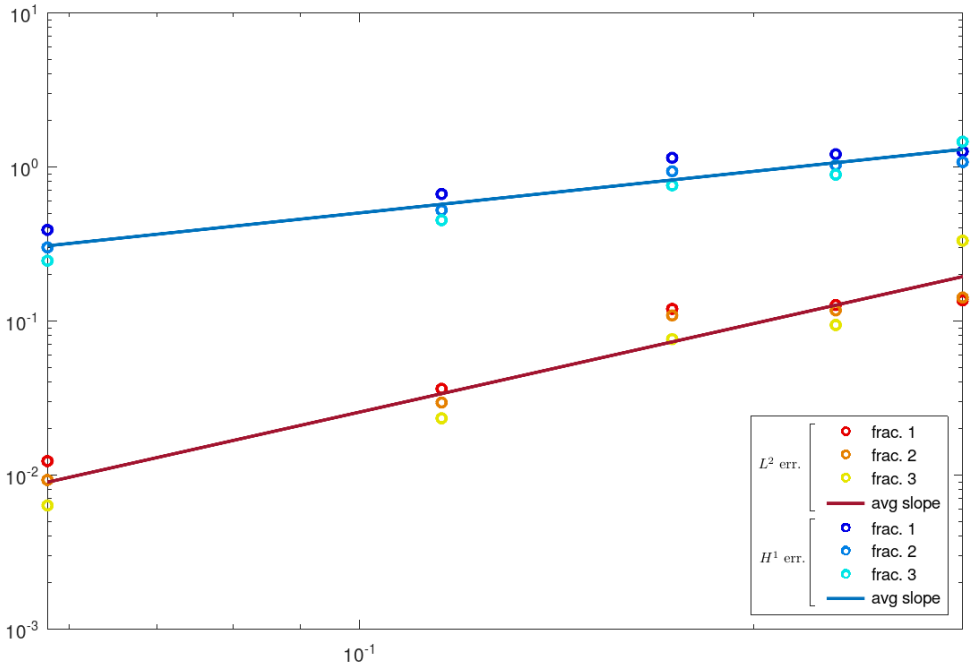

Figure 3.2. Convergence to the exact solution for Frac3 in L^2 and H^1 norms, for decreasing δ, for the three fractures and average convergence orders.

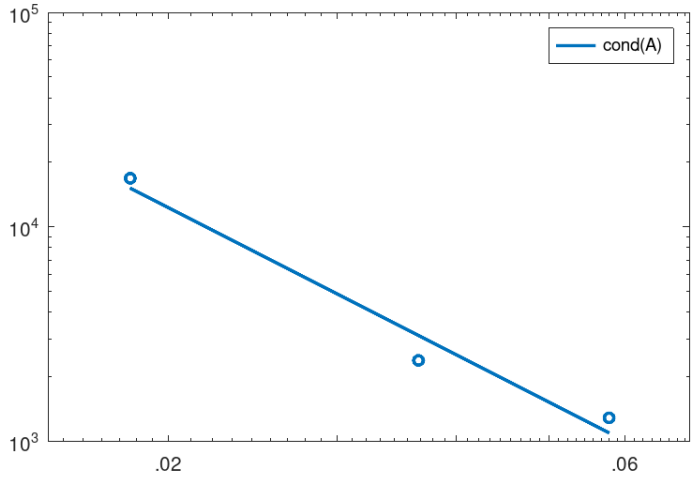

Figure 3.3. Condition number of A for Frac3 (points), for varying δ, and the corresponding trend line, with slope -2.28.

Chapter 4

Non-conforming optimization approach

To avoid the need for mesh conformity, a way of satisfying the conditions 1.4 and 1.5 on the traces other than the gluing of DOFs must be employed. One technique is to minimize a functional depending on the jump of the hydraulic head and the residual flux on the traces, constrained by the satisfaction of the flow equations on the fractures, as proposed in [7, 8]. The solution of the resulting optimal control problem can be carried out using gradient descent methods [7, 8] and parallel solvers can be efficiently implemented to handle simulations of large scale fracture networks [10]. In Section 4.2, a direct implementation is detailed instead, relying on the equivalence of the optimal control problem with Karush-Kuhn-Tucker (KKT) conditions, following [9].

4.1 Optimal control formulation

The problem of flow on a single fracture F_i can be stated, $\forall i \in \mathfrak{I}$, in a weak form multiplying equation 1.1 by a function $v \in V_i$ and integrating over F_i, obtaining, with a similar procedure to the one described in Section 1.3,

$$\textbf{Find } H_i \in V_i^D \text{ s.t.} \qquad \int_{F_i} \boldsymbol{K}_i \nabla H_i \nabla v \, \mathrm{d}\Omega - \sum_{S \in \mathcal{S}_i} \int_S \left[\!\left[\frac{\partial H_i}{\partial \nu_S^i} \right]\!\right] v_{|S} \, \mathrm{d}\Gamma = \\ = \int_{F_i} Q_i v \, \mathrm{d}\Omega + \int_{\Gamma_{iN}} G_{iN} v_{|\Gamma_{iN}} \, \mathrm{d}\Gamma, \quad \forall v \in V_i. \tag{4.1}$$

Following the approach of [7], let us first consider the case in which $\Gamma_{Di} \neq \emptyset$, for all $i \in \mathfrak{I}$. For each trace $S \in \mathcal{S}$, define the space $\mathcal{U}^S := H^{-\frac{1}{2}}(S)$ and define the spaces

$$\mathcal{U}^{\mathcal{S}_i} = \prod_{S \in \mathcal{S}_i} \mathcal{U}^S, \qquad \mathcal{U} = \prod_{i \in \mathfrak{I}} \mathcal{U}^{\mathcal{S}_i}.$$

Let $U_i^S \in \mathcal{U}^S$ and $U_j^S \in \mathcal{U}^S$ be variables, defined on each trace $S \in \mathcal{S}$, with $\{i, j\} = I_S$, respectively representing the jump of the co-normal derivatives of the hydraulic head $\left[\!\left[\frac{\partial H_i}{\partial \nu_S^i} \right]\!\right]$ and $\left[\!\left[\frac{\partial H_j}{\partial \nu_S^j} \right]\!\right]$, so that conditions 1.5 are equivalently stated as

$$U_i^{S_m} + U_j^{S_m} = 0 \quad \text{on } S_m \quad \forall m \in \mathfrak{M}, \quad \{i, j\} = I_{S_m},$$

Introducing the linear bounded operators $A_i \in \mathcal{L}(V_i, V_i')$, $A_i^D \in \mathcal{L}(V_i^D, V_i')$, $B_i \in \mathcal{L}(\mathcal{U}^{\mathcal{S}_i}, V_i')$ and $B_{iN} \in \mathcal{L}(H^{-\frac{1}{2}}(\Gamma_{iN}), V_i')$ defined such that

$$\begin{aligned}
\langle A_i w, v\rangle_{V_i',V_i} &= (\boldsymbol{K}_i \nabla w, \nabla v)_{F_i}, \quad w, v \in V_i \\
\langle A_i^D w, v\rangle_{V_i',V_i} &= (\boldsymbol{K}_i \nabla w, \nabla v)_{F_i}, \quad w \in V_i^D, v \in V_i \\
\langle B_i w, v\rangle_{V_i',V_i} &= \langle w, v_{|_{\mathcal{S}_i}}\rangle_{\mathcal{U}^{\mathcal{S}_i},\mathcal{U}^{\mathcal{S}_i}'}, \quad w \in \mathcal{U}^{\mathcal{S}_i}, v \in V_i \\
\langle B_{iN} w, v\rangle_{V_i',V_i} &= \langle w, v_{|_{\Gamma_{iN}}}\rangle_{H^{-\frac{1}{2}}(\Gamma_{iN}),H^{\frac{1}{2}}(\Gamma_{iN})}, \quad w \in H^{-\frac{1}{2}}(\Gamma_{iN}), v \in V_i
\end{aligned}$$

the form 4.1 is equivalent to

$$\textbf{Find } H_i^0 \in V_i \text{ s.t.} \qquad A_i H_i^0 = q_i + B_i U_i + B_{iN} G_{iN} - A_i^D H_i^D, \tag{4.2}$$

where $H_i = H_i^0 + H_i^D$, with $H_i^0 \in V_i$ and H_i^D is a lifting of the Dirichlet boundary condition on Γ_{iD}. Problem 4.2 is well-posed, provided that $\Gamma_{Di} \neq \emptyset$. For every trace $S \in \mathcal{S}$, define the space $\mathcal{H}^S := H^{\frac{1}{2}}(S)$. Let

$$\mathcal{H}^{\mathcal{S}_i} = \prod_{S \in \mathcal{S}_i} \mathcal{H}^S, \qquad \mathcal{H} = \prod_{i \in \mathfrak{I}} \mathcal{H}^{\mathcal{S}_i}.$$

Define the differentiable functional $J : \mathcal{U} \to \mathbb{R}$

$$J(U) := \frac{1}{2} \sum_{m \in \mathfrak{M}} \left(\left\| H_i(U_i)_{|_{S_m}} - H_j(U_j)_{|_{S_m}} \right\|^2_{\mathcal{H}^{S_m}} + \left\| U_i^{S_m} + U_j^{S_m} \right\|^2_{\mathcal{U}^{S_m}} \right),$$

where $\{i, j\} = I_{S_m}$ and $H_i(U_i)$ represents the solution of problem 4.2, given a particular choice of U_i, $i \in \mathfrak{I}$. Note that when the interface conditions 1.4 and 1.5 are satisfied, the functional $J(U)$ reaches its minimum $J(U) = 0$.

The problem 1.1-1.5 can be recast equivalently [7] as the optimal control problem

$$\begin{aligned}
\textbf{Find } U \in \mathcal{U} \text{ solution of} \quad & \min J(U) \\
& \text{s.t.} \quad A_i H_i^0 = q_i + B_i U_i + B_{iN} G_{iN} - A_i^D H_i^D \quad \forall i \in \mathfrak{I}.
\end{aligned} \tag{4.3}$$

From this point forward, a more general case will be considered, in which fractures are allowed to have Neumann boundary conditions on the entire boundary, as long as there is at least one fracture with Dirichlet boundary conditions on a nonempty portion of the boundary. To this aim introduce the real parameter $\alpha > 0$ [8] and redefine the control variables

$$U_i^S := \left[\!\left[\frac{\partial H_i}{\partial \boldsymbol{n}_S^i} \right]\!\right] + \alpha H_{i|_S} \tag{4.4}$$

The equations 4.2 retain the same form, but redefining the operators A_i and A_i^D as

$$\langle A_i w, v\rangle_{V_i',V_i} = (\boldsymbol{K}_i \nabla w, \nabla v)_{F_i} + \alpha (w_{|_{\mathcal{S}_i}}, v_{|_{\mathcal{S}_i}})_{\mathcal{S}_i}, \quad w, v \in V_i \tag{4.5}$$

$$\langle A_i^D w, v\rangle_{V_i',V_i} = (\boldsymbol{K}_i \nabla w, \nabla v)_{F_i} + \alpha (w_{|_{\mathcal{S}_i}}, v_{|_{\mathcal{S}_i}})_{\mathcal{S}_i}, \quad w \in V_i^D, v \in V_i \tag{4.6}$$

With the new operators, problem 4.2 is well-posed even in the pure Neumann case for non-isolated fractures [8]. The functional $J(U)$ is redefined as

$$\begin{aligned}
J(U) = \frac{1}{2} \sum_{m \in \mathfrak{M}} \Big(& \left\| H_i(U_i)_{|_{S_m}} - H_j(U_j)_{|_{S_m}} \right\|^2_{\mathcal{H}^{S_m}} + \\
& \left\| U_i^{S_m} + U_j^{S_m} - \alpha \Lambda_{\mathcal{H}^{S_m}} \left(H_i(U_i)_{|_{S_m}} + H_j(U_j)_{|_{S_m}} \right) \right\|^2_{\mathcal{U}^{S_m}} \Big),
\end{aligned} \tag{4.7}$$

where $\{i,j\} = I_{S_m}$ and $\Lambda_{\mathcal{H}^{S_m}} : \mathcal{H}^{S_m} \to \mathcal{H}^{S_m\prime}$ is the Riesz isomorphism between $\mathcal{H}^{S_m}$ and its dual. The minimization of the new functional 4.7 with the same constraints as in problem 4.3, but with the new operators 4.5 and 4.6, still results in the solution of the problem 1.1-1.5 [8].

4.2 Discrete formulation

For each fracture F_i, consider a mesh $\mathcal{T}_{\delta,i}$ on F_i and a mesh $\mathcal{T}^m_{\delta,i}$ on each trace $S_m \in \mathcal{S}_i$. Let $V^D_{\delta,i} \subset V^D_i$ be a finite-dimensional space generated by the basis functions $\varphi_{i,k}$, for $k = 1, \ldots, N^D_i = N_i + N_{i,D}$, defined on fracture F_i. Define also $V_{h,i} \subset V^D_{\delta,i}$ to be the space generated by the first N_i basis functions $\varphi_{i,k}$. In addition, let $W^m_{\delta,i} \subset L^2(S_m)$, for each $S_m \in \mathcal{S}_i$, be a finite-dimensional space generated by the basis functions $\psi^m_{i,k} \in L^2(S_m)$, for $k = 1, \ldots, N^m_i$. Define the discrete hydraulic head $h_i \in V^D_{\delta,i}$ and the discrete control variables $u^m_i \in W^m_{\delta,i}$, which can be represented as

$$h_i = \sum_{k=1}^{N^D_i} h_{i,k}\varphi_{i,k}, \qquad u^m_i = \sum_{k=1}^{N^m_i} u^m_{i,k}\psi^m_{i,k}.$$

The discrete variables are aggregated for the whole network giving

$$h := \prod_{i\in\mathfrak{I}} h_i \in V^D_\delta := \prod_{i\in\mathfrak{I}} V^D_{\delta,i}, \qquad u := \prod_{m\in\mathfrak{M}} (u^m_i, u^m_j) \in W_\delta := \prod_{m\in\mathfrak{M}} (W^m_{\delta,i} \times W^m_{\delta,j}),$$

where, in the expression of u, $\{i,j\} = I_{S_m}$, with $i < j$ to fix an order. Substituting the discrete variables in the expression of $J(U)$, changing the $\mathcal{H}^{S_m}$ and $\mathcal{U}^{S_m}$ norms with ones in $L^2(S_m)$ and writing them explicitly, one obtains the discrete cost functional

$$\begin{aligned}
J(u) = \frac{1}{2}\sum_{m\in\mathfrak{M}} \Bigg\{ & \int_{S_m} \left[\sum_{k=1}^{N^D_i} h_{i,k}\varphi_{i,k|_{S_m}} - \sum_{k=1}^{N^D_j} h_{j,k}\varphi_{j,k|_{S_m}}\right]^2 \mathrm{d}\gamma + \\
& \int_{S_m} \left[\sum_{k=1}^{N_{i,m}} u^m_{i,k}\psi^m_{i,k} + \sum_{k=1}^{N_{j,m}} u^m_{j,k}\psi^m_{j,k} - \alpha\left(\sum_{k=1}^{N^D_i} h_{i,k}\varphi_{i,k|_{S_m}} + \sum_{k=1}^{N^D_j} h_{j,k}\varphi_{j,k|_{S_m}}\right)\right]^2 \mathrm{d}\gamma \Bigg\} \\
= \frac{1}{2}\sum_{m\in\mathfrak{M}} \Bigg\{ & \sum_{i\in I_{S_m}} \sum_{k,l=1}^{N^D_i} h_{i,k}h_{i,l}(\alpha^2+1)(\varphi_{i,k|_{S_m}}, \varphi_{i,l|_{S_m}})_{S_m} + \\
& 2\sum_{k=1}^{N^D_i}\sum_{l=1}^{N^D_j} h_{i,k}h_{j,l}(\alpha^2-1)(\varphi_{i,k|_{S_m}}, \varphi_{j,l|_{S_m}})_{S_m} + \\
& \sum_{i\in I_{S_m}} \sum_{k,l=1}^{N_{i,m}} u^m_{i,k}u^m_{i,l}(\psi^m_{i,k}, \psi^m_{i,l})_{S_m} + 2\sum_{k=1}^{N_{i,m}}\sum_{l=1}^{N_{j,m}} u^m_{i,k}u^m_{j,l}(\psi^m_{i,k}, \psi^m_{j,l})_{S_m} + \\
& - 2\alpha \sum_{i\in I_{S_m}} \sum_{k=1}^{N_{i,m}}\sum_{l=1}^{N^D_i} u^m_{i,k}h_{i,l}(\psi^m_{i,k}, \varphi_{i,l|_{S_m}})_{S_m} - 2\alpha \sum_{\substack{i,j\in I_{S_m}\\ i\neq j}} \sum_{k=1}^{N_{i,m}}\sum_{l=1}^{N^D_j} u^m_{i,k}h_{j,l}(\psi^m_{i,k}, \varphi_{j,l|_{S_m}})_{S_m} \Bigg\},
\end{aligned}$$

where, in every sum in which indices i and j are not defined, it is meant $\{i,j\} = I_{S_m}$. Introduce, with the same notation as for the discrete variables, the vectors of their coefficients

$$h_i = (h_{i,1}, \dots, h_{i,N_i^D})^T \in \mathbb{R}^{N_i^D}, \qquad h = (h_1, \dots, h_{\#\mathfrak{I}})^T \in \mathbb{R}^{N_{\mathcal{F}}},$$

with $N_{\mathcal{F}} = \sum_{i\in\mathfrak{I}} N_i^D$. For the control variables, on each trace S_m, with $\{i,j\} = I_{S_m}$, $i<j$, denote respectively with '$-$' and '$+$' the variables, the coefficients and the basis functions on S_m related to fractures F_i and F_j. In this context, define also $N_-^m = N_i^m$ and $N_+^m = N_j^m$. The resulting vectors are

$$\begin{aligned} u_*^m &= (u_{*,1}^m, \dots, u_{*,N_*^m}^m)^T \in \mathbb{R}^{N_*^m}, \text{ for } * \in \{-,+\}, \\ u^m &= (u_-^m, u_+^m)^T, \qquad u = (u^1, \dots, u^{\#\mathfrak{M}}) \in \mathbb{R}^{N^{\mathcal{S}}}, \end{aligned}$$

with $N^{\mathcal{S}} = \sum_{m\in\mathfrak{M}} (N_-^m + N_+^m)$. Furthermore, define the map $\mathcal{I} : \mathfrak{M} \times \{-,+\} \to \mathfrak{I}$ defined as $\mathcal{I}(m,-) = i$, $\mathcal{I}(m,+) = j$, with $\{i,j\} = I_{S_m}$, $i<j$, giving the index of the fracture to which a trace quantity, identified by the index $m \in \mathfrak{M}$ and the symbol $* \in \{-,+\}$, is associated. Define also the set $J_i \subset \mathfrak{I}$, $\forall i \in \mathfrak{I}$, of the indices of the fractures sharing a trace with F_i. The functional $J(u)$ can then be expressed through appropriate matrices as

$$\begin{aligned} J(u) = \frac{1}{2}\Bigg\{ & \sum_{i\in\mathfrak{I}} \left[h_i^T \mathbb{G}_{ii}^h h_i + 2 \sum_{j\in J_i} h_i^T \mathbb{G}_{ij}^h h_j \right] + \\ & \sum_{m\in\mathfrak{M}} \left[(u_-^m)^T \mathbb{G}_{m,-}^u u_-^m + (u_+^m)^T \mathbb{G}_{m,+}^u u_+^m - 2(u_+^m)^T \mathbb{G}_{m,\pm}^u u_-^m \right] + \\ & - 2\alpha \sum_{m\in\mathfrak{M}} \left[(u_-^m)^T \mathbb{B}_-^m h_{\mathcal{I}(m,-)} + (u_+^m)^T \mathbb{B}_+^m h_{\mathcal{I}(m,+)} + u_-^m \mathbb{B}_{\mp}^m h_{\mathcal{I}(m,+)} + u_+^m \mathbb{B}_{\pm}^m h_{\mathcal{I}(m,-)} \right] \Bigg\} \\ = & \frac{1}{2} h^T \mathbb{G}^h h + \frac{1}{2} u^T \mathbb{G}^u u - \alpha u^T \mathbb{B} h, \end{aligned}$$

where $\mathbb{G}^h = (\mathbb{G}_{ij}^h)_{i\in\mathfrak{I}, j\in J_i\cup\{i\}}$, with

$$\begin{aligned} (\mathbb{G}_{ii}^h)_{kl} &= (\alpha^2+1) \sum_{S_m\in\mathcal{S}_i} (\varphi_{i,k|_{S_m}}, \varphi_{i,l|_{S_m}})_{S_m}, \quad \forall i \in \mathfrak{I} \\ (\mathbb{G}_{ij}^h)_{kl} &= (\alpha^2-1)(\varphi_{i,k|_{S_m}}, \varphi_{j,l|_{S_m}})_{S_m}, \quad \text{with } \{i,j\} = I_{S_m}, \forall m \in \mathfrak{M}, \end{aligned}$$

and $\mathbb{G}^u = \mathrm{diag}(\mathbb{G}_1^u, \dots, \mathbb{G}_{\#\mathfrak{M}}^u)$, with, $\forall m \in \mathfrak{M}$,

$$\mathbb{G}_m^u = \begin{bmatrix} \mathbb{G}_{m,-}^u & \mathbb{G}_{m,\pm}^u \\ (\mathbb{G}_{m,\pm}^u)^T & \mathbb{G}_{m,+}^u \end{bmatrix},$$

$$\begin{aligned} (\mathbb{G}_{m,*}^u)_{kl} &= (\psi_{*,k}^m, \psi_{*,l}^m)_{S_m}, \quad * \in \{-,+\} \\ (\mathbb{G}_{m,\pm}^u)_{kl} &= (\psi_{-,k}^m, \psi_{+,l}^m)_{S_m}. \end{aligned}$$

The matrix $\mathbb{B}$ is constructed block-wise as

$$\begin{aligned} \mathbb{B}_{im} &= \begin{bmatrix} \mathbb{B}_-^m & \mathbb{B}_\pm^m \end{bmatrix} \in \mathbb{R}^{N_-^m \times (N_-^m + N_+^m)}, \quad \text{with } i = \mathcal{I}(m,-), \quad \forall m \in \mathfrak{M}, \\ \mathbb{B}_{im} &= \begin{bmatrix} \mathbb{B}_\mp^m & \mathbb{B}_+^m \end{bmatrix} \in \mathbb{R}^{N_+^m \times (N_-^m + N_+^m)}, \quad \text{with } i = \mathcal{I}(m,+), \quad \forall m \in \mathfrak{M}, \end{aligned}$$

where

$$
\begin{aligned}
(\mathbb{B}_{*}^{m})_{kl} &= (\psi_{i,k}^{m}, \varphi_{i,l|_{S_m}})_{S_m}, \quad \text{with } i = \mathcal{I}(m,*),\ * \in \{-,+\},\\
(\mathbb{B}_{\mp}^{m})_{kl} &= (\psi_{i,k}^{m}, \varphi_{j,l|_{S_m}})_{S_m}, \quad \text{with } i = \mathcal{I}(m,-),\ j = \mathcal{I}(m,+),\\
(\mathbb{B}_{\pm}^{m})_{kl} &= (\psi_{j,k}^{m}, \varphi_{i,l|_{S_m}})_{S_m}, \quad \text{with } i = \mathcal{I}(m,-),\ j = \mathcal{I}(m,+).
\end{aligned}
$$

The minimization problem can be written as

$$
\begin{aligned}
\min_{w} \ & \frac{1}{2} w^T \mathbb{G} w \\
\text{s.t.} \ & Cw = \tilde{q}
\end{aligned}
\tag{4.8}
$$

where

$$
\mathbb{G} = \begin{bmatrix} \mathbb{G}^h & -\alpha \mathbb{B}^T \\ -\alpha \mathbb{B} & \mathbb{G}^u \end{bmatrix} \in \mathbb{R}^{(N^{\mathcal{F}}+N^{\mathcal{S}})\times(N^{\mathcal{F}}+N^{\mathcal{S}})}, \quad w = \begin{bmatrix} h \\ u \end{bmatrix} \in \mathbb{R}^{N^{\mathcal{F}}+N^{\mathcal{S}}},
$$

$$
\begin{aligned}
C &= \begin{bmatrix} A & -B \end{bmatrix} \in \mathbb{R}^{N^{\mathcal{F}}\times(N^{\mathcal{F}}+N^{\mathcal{S}})},\\
A &= \operatorname{diag}(A_1, \dots, A_{\#\mathfrak{I}}) \in \mathbb{R}^{N^{\mathcal{F}}\times N^{\mathcal{F}}},\\
(A_i)_{kl} &= \begin{cases} (\boldsymbol{K}_i \nabla\varphi_{i,l}, \nabla\varphi_{i,k})_{F_i} + \alpha \sum_{S\in\mathcal{S}_i} (\varphi_{i,l|_S}, \varphi_{i,k|_S})_S & \text{if } k,l \in \mathcal{N}_i \\ 1 & \text{if } k = l \in \mathcal{N}_{i,D} \\ 0 & \text{otherwise} \end{cases},
\end{aligned}
$$

with $\mathcal{N}_i := \{1, \dots, N_i\}$, $\mathcal{N}_{i,D} := \{N_i + 1, \dots, N_i^D\}$. The matrix $B \in \mathbb{R}^{N^{\mathcal{F}}\times N^{\mathcal{S}}}$ is constructed blockwise as

$$
\begin{aligned}
B_{im} &= \begin{bmatrix} \mathbb{B}_{-}^{m} & 0 \end{bmatrix} \in \mathbb{R}^{N_{-}^{m}\times(N_{-}^{m}+N_{+}^{m})}, \quad \text{with } i = \mathcal{I}(m,-), \quad \forall m \in \mathfrak{M},\\
B_{im} &= \begin{bmatrix} 0 & \mathbb{B}_{+}^{m} \end{bmatrix} \in \mathbb{R}^{N_{+}^{m}\times(N_{-}^{m}+N_{+}^{m})}, \quad \text{with } i = \mathcal{I}(m,+), \quad \forall m \in \mathfrak{M}.
\end{aligned}
$$

The term $\tilde{q} = q - A^D h^D \in \mathbb{R}^{N^{\mathcal{F}}}$ accounts for the forcing term and the boundary condition terms of equation 4.2, where $G_{iN} = 0\ \forall i \in \mathfrak{I}$, corresponding to homogeneous Neumann boundary conditions on Γ_N. In particular

$$
A^D = \operatorname{diag}(A_1^D, \dots, A_{\#\mathfrak{I}}^D) \in \mathbb{R}^{N^{\mathcal{F}}\times N^{\mathcal{F}}}, \quad h^D = \begin{bmatrix} h_1^D \\ \vdots \\ h_{\#\mathfrak{I}}^D \end{bmatrix} \in \mathbb{R}^{N^{\mathcal{F}}\times N^{\mathcal{F}}}
$$

$$
(A_i^D)_{kl} = \begin{cases} (\boldsymbol{K}_i \nabla\varphi_{i,l}, \nabla\varphi_{i,k})_{F_i} + \alpha \sum_{S\in\mathcal{S}_i} (\varphi_{i,l|_S}, \varphi_{i,k|_S})_S & \text{if } k \in \mathcal{N}_i, l \in \mathcal{N}_{i,D} \\ 1 & \text{if } k = l \in \mathcal{N}_{i,D} \\ 0 & \text{otherwise} \end{cases},
$$

and $(h_i^D)_k$ are the coefficients of the lifting of the Dirichlet boundary conditions on fracture F_i in the basis of $V_{\delta,i}^D$.

The minimization problem 4.8 is equivalent to the KKT conditions

$$
\begin{bmatrix} \mathbb{G} & C^T \\ C & 0 \end{bmatrix} \begin{bmatrix} w^* \\ -p^* \end{bmatrix} = \begin{bmatrix} 0 \\ \tilde{q} \end{bmatrix}
\tag{4.9}
$$

where we call

$$
\mathcal{A} = \begin{bmatrix} \mathbb{G} & C^T \\ C & 0 \end{bmatrix} \in \mathbb{R}^{(2N^{\mathcal{F}}+N^{\mathcal{S}})\times(2N^{\mathcal{F}}+N^{\mathcal{S}})}.
$$

4.3 Numerical results

The approach described in this Chapter is tested on the two DFNs Frac3 and Frac36 introduced in section 3.3. All tests were conducted with the choice $\alpha = 1$ and using first order FEM approximations on fractures and traces. The mesh size parameters are expressed as a fraction of the square root of the average fracture area of the DFN.

Convergence results are presented in Figure 4.1 for Frac3. The discretization parameter δ controls the length of the segments of the trace meshes, while the areas of the triangles of the fracture meshes are smaller than δ^2. The L^2 error shows an average convergence rate of 2.07, while the H^1 error decreases with a rate of 0.94, in agreement with the standard FEM estimates. The value of the errors are very similar to those shown in Figure 3.2 obtained with the conforming approach for the same values of δ.

Figure 4.3 shows results for Frac3 and Frac36. The two tests differ in the distribution of traces' lengths: Frac3 presents traces of practically uniform length, while Frac36 contains traces of wide ranging lengths. Two discretization parameters are used: δ_H controls the square root of the areas of the elements in the domains' meshes, while δ_U determines the lengths of the elements in the traces' meshes. The value of δ_H is fixed for each test, while δ_U is allowed to vary. For Frac3, the condition number of the KKT matrix $\mathcal{A}$ decreases for increasing values of the ratio $\frac{\delta_U}{\delta_H}$, while for Frac36 it stagnates for values of $\frac{\delta_U}{\delta_H}$ grater than 2 (Figure 4.3 a-b). An interpretation of the different behaviour between the two tests can be given observing that in the case of Frac36, a fraction of the traces are so short that even with the smallest choice of δ_U, their mesh is constituted by a single segment and cannot be made any coarser. Denote the fraction of such traces by n_C. Increasing δ_U, a bigger fraction of traces falls into this group (Figure 4.3 d). In the case of Frac3, no trace reaches this condition with the range of values of δ_U used in the test (Figure 4.3 c). Greater values of δ_U result in an increase in both the flux mismatch $H^{-\frac{1}{2}}$ norms (Figure 4.3 e-f) and the hydraulic head jump L^2 norms (Figure 4.3 g-h) on the traces. The $H^{-\frac{1}{2}}$ norm of the flux mismatch is approximated as [6]

$$\left\| u_i^m + u_j^m - \alpha(h_{i|_{S_m}} + h_{j|_{S_m}}) \right\|_{H^{-\frac{1}{2}}(S_m)} \approx \left(\sum_{k=1}^{N^m} |\Lambda_k^m| \left\| u_i^m + u_j^m - \alpha(h_{i|_{S_m}} + h_{j|_{S_m}}) \right\|^2_{L^2(\Lambda_k^m)} \right)^{\frac{1}{2}},$$

where Λ_k^m are the N^m segments resulting from the union of the nodes of the two meshes $\mathcal{T}_{i,\delta_U}^m$ and $\mathcal{T}_{j,\delta_U}^m$ and $|\Lambda_k^m|$ is the length of Λ_k^m. All $H^{-1/2}$ norms on the traces are re-scaled with the sum of the lengths of all the traces in the DFN.

Figure 4.2 reports the dependence of the condition number of $\mathcal{A}$ on δ_H for the test Frac3. The study is shown for different choices of $\frac{\delta_U}{\delta_H}$. The condition number diverges approximately as δ_H^{-2}. The value of $\frac{\delta_U}{\delta_H}$ influences the value of the condition number as illustrated in Figure 4.3, but it does not impact significantly the steepness of the slope. The condition number of $\mathcal{A}$ is much higher than the one of the stiffness matrix involved in the conforming approach (Figure 3.3) for the same values of δ_H, in particular for small values of $\frac{\delta_U}{\delta_H}$.

Figure 4.4 and 4.5 show the convergence of the average flux mismatch and hydraulic head jump norms on traces for the tests Frac3 and Frac36, respectively, with different choices of $\frac{\delta_U}{\delta_H}$. The corresponding slope values are reported in Table 4.1. In the case of

Frac36, the convergence appears to be slower for higher $\frac{\delta_U}{\delta_H}$, for both the flux mismatch and the hydraulic head jump. In particular for the flux mismatch, this is possibly due to the presence of short traces, for which the decrease in prescribed mesh size does not result in a refinement in the explored range of δ_U. Indeed, the fraction of traces which are never refined in this convergence study for Frac36, for the three choices of $\frac{\delta_U}{\delta_H} = .5,2,4$, are 0.03, 0.25, 0.49, respectively.

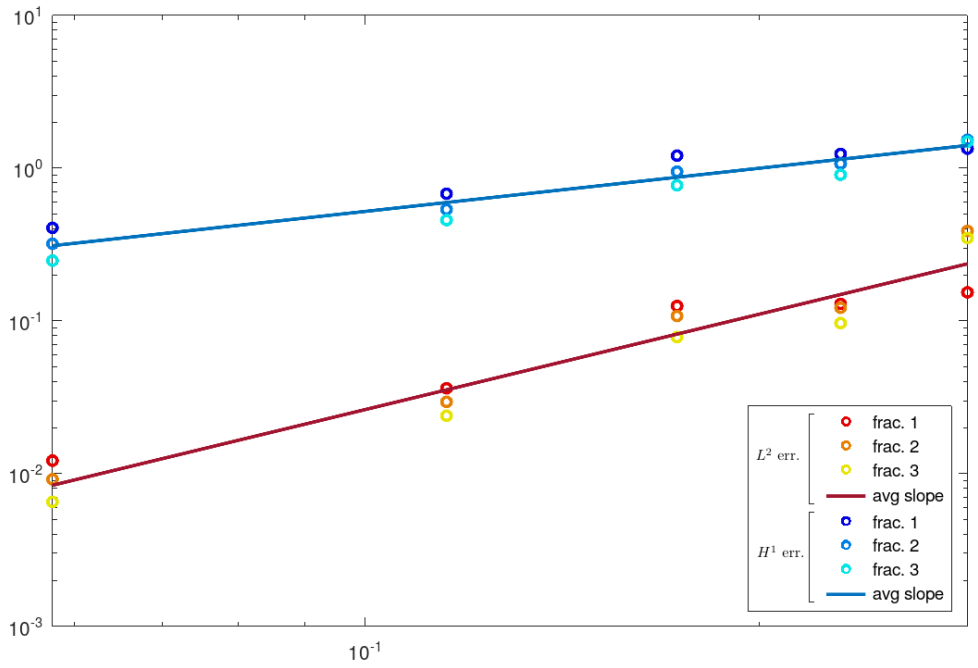

Figure 4.1. Convergence to the exact solution for Frac3 in L^2 and H^1 norms, for decreasing δ, for the three fractures and average convergence orders.

	$\frac{\delta_U}{\delta_H}$	.5	2	4
Frac3	flux	1.5817	1.5477	1.0868
	head	1.3766	1.5952	1.3073
Frac36	flux	1.3082	1.1735	0.9151
	head	0.6051	0.5495	0.3099

Table 4.1. Convergence slopes of the average flux mismatch and hydraulic head jump norms on traces, for Frac3 and Frac36.

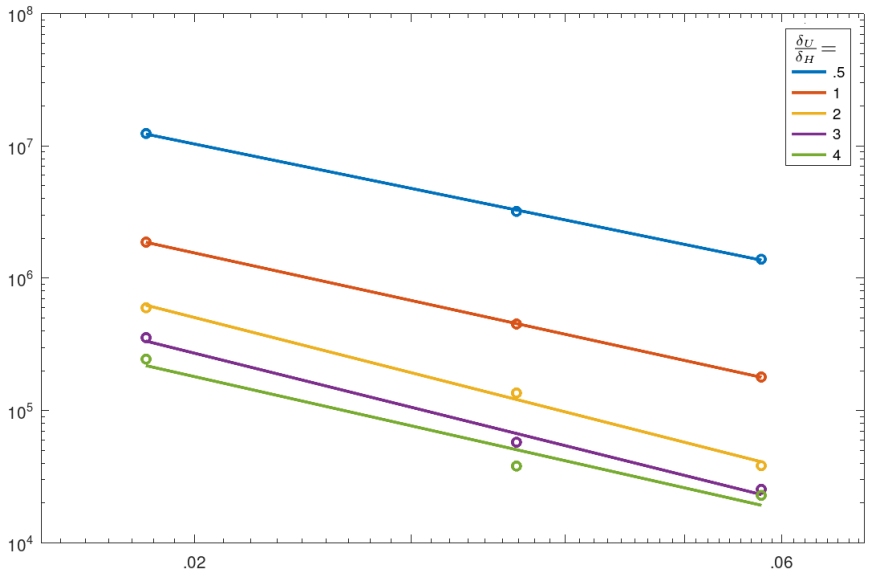

Figure 4.2. Condition number of $\mathcal{A}$ for Frac3 (points), for varying δ_H, and the corresponding slope lines. The results are shown for values of $\frac{\delta_U}{\delta_H} = .5, 1, 2, 3, 4$. The average slope is -2.15

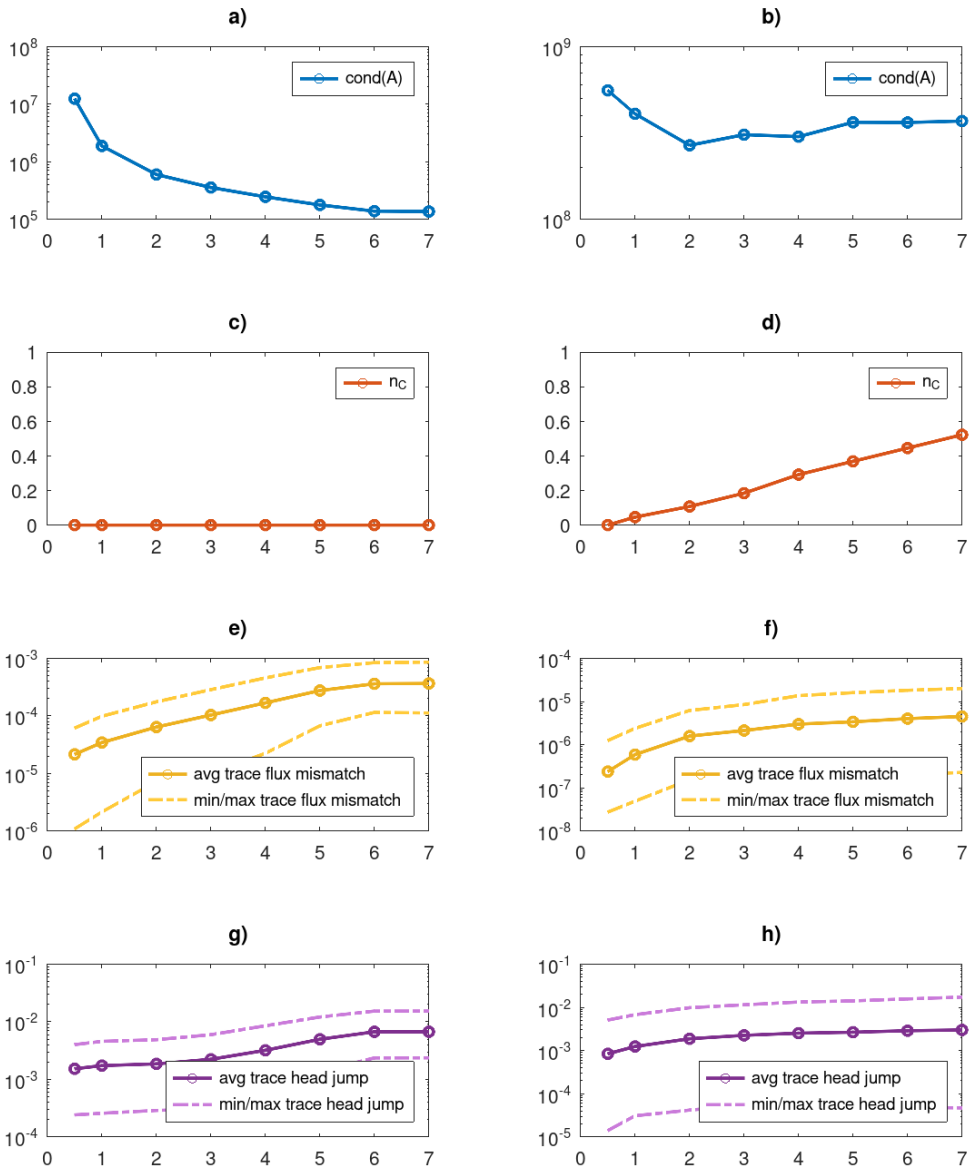

Figure 4.3. From the top, condition number of $\mathcal{A}$, trace mesh size, hydraulic head jump and flux mismatch norms, plotted against varying values of the ratio $\frac{\delta_U}{\delta_H}$, for Frac3 with $\delta_H = 1.8 \cdot 10^{-2}$ on the left and Frac36 with $\delta_H = 2.8 \cdot 10^{-2}$ on the right.

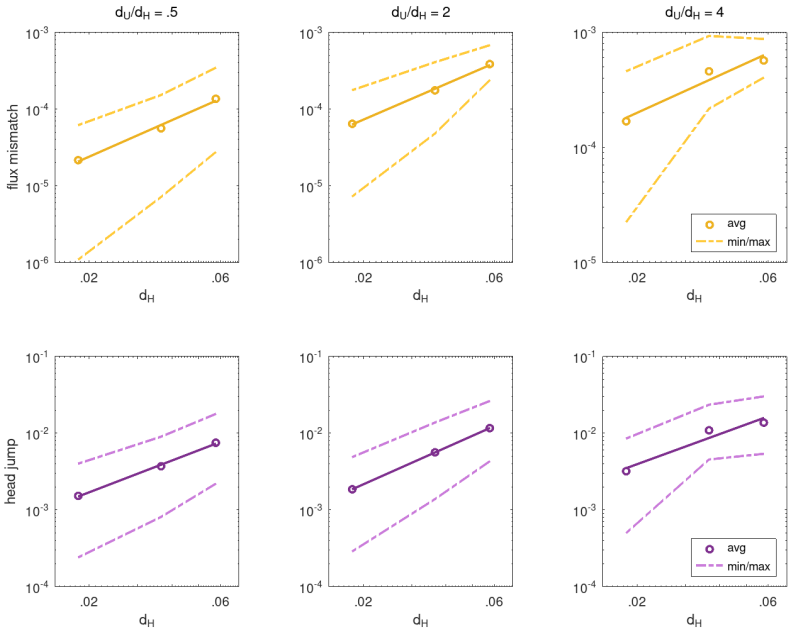

Figure 4.4. Average flux mismatch (top) and hydraulic head jump (bottom) for Frac3, for varying δ_H, and the corresponding slope lines. The results are shown for values of $\frac{\delta_U}{\delta_H} = .5, 2, 4$.

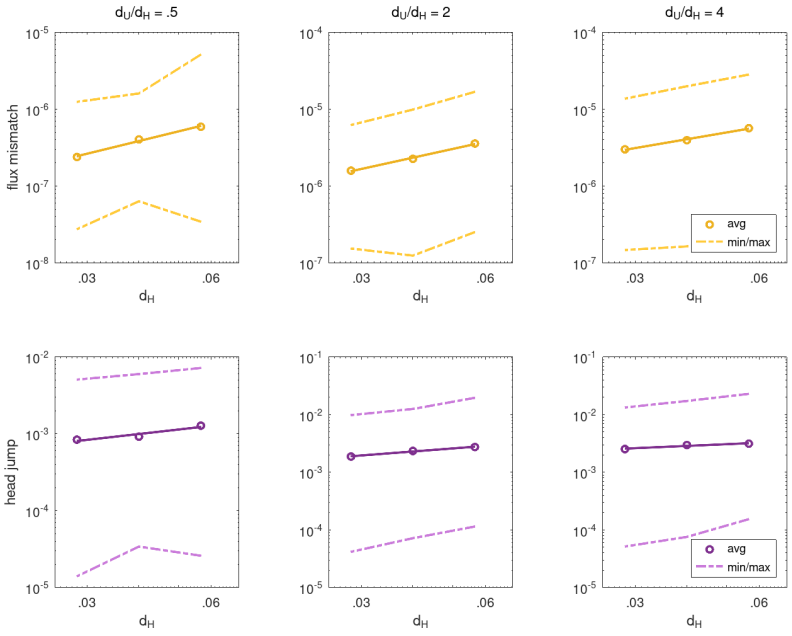

Figure 4.5. Average flux mismatch (top) and hydraulic head jump (bottom) for Frac36, for varying δ_H, and the corresponding slope lines. The results are shown for values of $\frac{\delta_U}{\delta_H} = .5, 2, 4$.

Chapter 5

Joint approach

The analysis of the two approaches described in the preceding Chapters suggests that combining them, the respective drawbacks could be ameliorated. Indeed, consider a partition of the domain into groups of fractures. The conforming VEM approach can be used within each group, while the optimization approach can be used to satisfy the continuity conditions at the intersections between fractures belonging to different groups. This joint technique could be used to exclude from the optimization short traces, which are associated with a higher condition number of the KKT matrix $\mathcal{A}$. On the other hand it could be useful to exclude some traces from the conforming process to allow the conforming meshes to have better properties near the traces. Furthermore, the use of the optimization approach between fracture groups could still allow a natural parallel implementation of the method. In the following, a possible formulation of this approach is proposed and the core idea for a direct implementation analogous to that of Section 4.2 is given. Strategies for a useful decomposition of the domain in fracture groups are not investigated here and are left for future discussion.

5.1 Optimal control formulation

Consider a partition of the domain Ω into groups of fractures $\mathcal{G}_i = \bigcup_{j\in J_i} F_j$, with $J_i \subseteq \mathfrak{I}$ the set of indices of the fractures composing the group $\mathcal{G}_i$, for $i \in \mathfrak{G}$ the fracture groups' indices, with $\mathfrak{G}$ of cardinality $\#\mathfrak{G}$. Let $\Gamma_{\mathcal{G}_i} = \Gamma_{\mathcal{G}_i D} \cup \Gamma_{\mathcal{G}_i N}$ be the boundary of $\mathcal{G}_i$, where $\Gamma_{\mathcal{G}_i D} = \bigcup_{j\in J_i} \Gamma_{jD}$ is the boundary with Dirichlet boundary condition and $\Gamma_{\mathcal{G}_i N} = \bigcup_{j\in J_i} \Gamma_{jN}$ the one with Neumann boundary conditions. For each fracture group $\mathcal{G}_i$, $i \in \mathfrak{G}$, define

$$\mathcal{S}^{\text{ext}}_{\mathcal{G}_i} := \{S = (F_k \cap F_l) : F_k \subseteq \mathcal{G}_i,\ F_l \not\subset \mathcal{G}_i\}$$

the set of traces produced by the intersections of fractures in the group $\mathcal{G}_i$ with those contained in other groups and

$$\mathcal{S}^{\text{int}}_{\mathcal{G}_i} := \{S = (F_k \cap F_l) : F_k, F_l \subseteq \mathcal{G}_i\}$$

the set of intersections between fractures both in group $\mathcal{G}_i$. Furthermore, let $\hat{\mathcal{S}}^{\text{int}}_{\mathcal{G}_i} \subseteq \mathcal{S}^{\text{int}}_{\mathcal{G}_i}$ be a possibly empty subset of $\mathcal{S}^{\text{int}}_{\mathcal{G}_i}$, and $\hat{\mathcal{S}}_{\mathcal{G}_i} := \mathcal{S}^{\text{ext}}_{\mathcal{G}_i} \cup \hat{\mathcal{S}}^{\text{int}}_{\mathcal{G}_i}$. Define the sets

$$\mathcal{S}^{\text{ext}}_{\mathcal{G}} := \bigcup_{i\in\mathfrak{G}} \mathcal{S}^{\text{ext}}_{\mathcal{G}_i}, \quad \hat{\mathcal{S}}^{\text{int}}_{\mathcal{G}} := \bigcup_{i\in\mathfrak{G}} \hat{\mathcal{S}}^{\text{int}}_{\mathcal{G}_i}, \quad \mathcal{S}^{\text{int}}_{\mathcal{G}} := \bigcup_{i\in\mathfrak{G}} \mathcal{S}^{\text{int}}_{\mathcal{G}_i}, \quad \hat{\mathcal{S}}_{\mathcal{G}} := \bigcup_{i\in\mathfrak{G}} \hat{\mathcal{S}}_{\mathcal{G}_i}.$$

Let also $F(S,-)$ and $F(S,+)$, with $S \in \mathcal{S}_{\mathcal{G}}^{\text{int}}$, denote the two fractures, both belonging to the same group, generating the trace S. Define the spaces

$$V_{\mathcal{G}_i} = H_0^1(\mathcal{G}_i) = \left\{ v \in \prod_{j \in J_i} V_j : \quad (v_{|_{F(S,-)}})_{|_S} = (v_{|_{F(S,+)}})_{|_S}, \, \forall S \in \mathcal{S}_{\mathcal{G}_i}^{\text{int}} \setminus \hat{\mathcal{S}}_{\mathcal{G}_i}^{\text{int}} \right\}$$

and

$$V_{\mathcal{G}_i}^D = H_D^1(\mathcal{G}_i) = \left\{ v \in \prod_{j \in J_i} V_j^D : \quad (v_{|_{F(S,-)}})_{|_S} = (v_{|_{F(S,+)}})_{|_S}, \, \forall S \in \mathcal{S}_{\mathcal{G}_i}^{\text{int}} \setminus \hat{\mathcal{S}}_{\mathcal{G}_i}^{\text{int}} \right\},$$

so that for each group $\mathcal{G}_i$, $i \in \mathfrak{G}$, the hydraulic head is

$$H_{\mathcal{G}_i} = \prod_{j \in J_i} H_j \in V_{\mathcal{G}_i}^D.$$

Analogously to the procedure of Section 4.1, the problem of flow on a group of fractures $\mathcal{G}_i$ can be stated, $\forall i \in \mathfrak{G}$, in a weak form multiplying equation 1.1 by a function $v \in V_{\mathcal{G}_i}$ and integrating over $\mathcal{G}_i$, obtaining,

$$\begin{aligned} &\textbf{Find } H_{\mathcal{G}_i} \in V_{\mathcal{G}_i}^D \text{ s.t.} \\ &\sum_{F_l \subseteq \mathcal{G}_i} \int_{F_l} \boldsymbol{K}_l \nabla H_l \nabla v_{|_{F_l}} \, \mathrm{d}\Omega - \sum_{S \in \mathcal{S}_{\mathcal{G}_i}^{\text{ext}}} \int_S \left[\!\!\left[\frac{\partial H_{\mathcal{G}_i}}{\partial \nu_S^{\mathcal{G}_i}} \right]\!\!\right] v_{|_S} \, \mathrm{d}\Gamma \\ &\qquad - \sum_{S \in \hat{\mathcal{S}}_{\mathcal{G}_i}^{\text{int}}} \sum_{* \in \{-,+\}} \int_S \left[\!\!\left[\frac{\partial H_{F(S,*)}}{\partial \nu_S^{F(S,*)}} \right]\!\!\right] v_{|_S} \, \mathrm{d}\Gamma = \\ &\qquad = \sum_{F_l \subseteq \mathcal{G}_i} \int_{F_l} Q_l v_{|_{F_l}} \, \mathrm{d}\Omega + \sum_{F_l \subseteq \mathcal{G}_i} \int_{\Gamma_{lN}} G_{lN} v_{|_{\Gamma_{lN}}} \, \mathrm{d}\Gamma, \quad \forall v \in V_{\mathcal{G}_i}, \end{aligned} \tag{5.1}$$

where the directional derivatives are meant along a unit vector co-normal to the given trace S, lying in the plane of the appropriate fracture.

For each trace $S \in \mathcal{S}_{\mathcal{G}_i}^{\text{ext}}$, given by the intersection of two fractures, one belonging to $\mathcal{G}_i$ and the other to a different group $\mathcal{G}_j$, define the control variables

$$U_{\mathcal{G}_i}^S \in \mathcal{U}^S, \quad U_{\mathcal{G}_j}^S \in \mathcal{U}^S,$$

with $\mathcal{U}^S := H^{-\frac{1}{2}}(S)$ as in Section 4.1. For each trace $S \in \hat{\mathcal{S}}_{\mathcal{G}}^{\text{int}}$, which is given instead by the intersection of the two fractures $F(S,-)$ and $F(S,+)$, both belonging to $\mathcal{G}_i$, define the control variables

$$U_{\mathcal{G}_i,\text{int}}^{S,-} \in \mathcal{U}^S, \quad U_{\mathcal{G}_i,\text{int}}^{S,+} \in \mathcal{U}^S.$$

Define the spaces

$$\mathcal{U}^{\hat{\mathcal{S}}_{\mathcal{G}_i}} = \left(\prod_{S \in \mathcal{S}_{\mathcal{G}_i}^{\text{ext}}} \mathcal{U}^S \right) \times \left(\prod_{S \in \hat{\mathcal{S}}_{\mathcal{G}_i}^{\text{int}}} (\mathcal{U}^S \times \mathcal{U}^S) \right), \qquad \hat{\mathcal{U}} = \prod_{i \in \mathfrak{G}} \mathcal{U}^{\hat{\mathcal{S}}_{\mathcal{G}_i}}.$$

For each fracture group define

$$U_{\mathcal{G}_i} = \left(\prod_{S \in \mathcal{S}_{\mathcal{G}_i}^{\text{ext}}} U_{\mathcal{G}_i}^S \right) \times \left(\prod_{S \in \hat{\mathcal{S}}_{\mathcal{G}_i}^{\text{int}}} (U_{\mathcal{G}_i,\text{int}}^{S,-} \times U_{\mathcal{G}_i,\text{int}}^{S,+}) \right) \in \mathcal{U}^{\hat{\mathcal{S}}_{\mathcal{G}_i}}.$$

Define also

$$\hat{U} = \prod_{i \in \mathfrak{G}} U_{\mathcal{G}_i} \in \hat{\mathcal{U}}.$$

The functional $J(U)$ introduced in 4.7 is now redefined as

$$\begin{aligned}
\hat{J}(\hat{U}) = \frac{1}{2} \sum_{S \in \mathcal{S}_{\mathcal{G}}^{\text{ext}}} \Bigg(& \left\| H_{\mathcal{G}_i}(U_{\mathcal{G}_i})_{|S} - H_{\mathcal{G}_j}(U_{\mathcal{G}_j})_{|S} \right\|_{\mathcal{H}^S}^2 + \\
& \left\| U_{\mathcal{G}_i}^S + U_{\mathcal{G}_j}^S - \alpha \Lambda_{\mathcal{H}^S} \left(H_{\mathcal{G}_i}(U_{\mathcal{G}_i})_{|S} + H_{\mathcal{G}_j}(U_{\mathcal{G}_j})_{|S} \right) \right\|_{\mathcal{U}^S}^2 \Bigg) + \\
\frac{1}{2} \sum_{S \in \hat{\mathcal{S}}_{\mathcal{G}}^{\text{int}}} \Bigg(& \left\| \left[H_{\mathcal{G}_i}(U_{\mathcal{G}_i})_{|_{F(S,-)}} \right]_{|S} - \left[H_{\mathcal{G}_i}(U_{\mathcal{G}_i})_{|_{F(S,+)}} \right]_{|S} \right\|_{\mathcal{H}^S}^2 + \\
& \left\| U_{\mathcal{G}_i,\text{int}}^{S,-} + U_{\mathcal{G}_i,\text{int}}^{S,+} - \alpha \Lambda_{\mathcal{H}^S} \left(\left[H_{\mathcal{G}_i}(U_{\mathcal{G}_i})_{|_{F(S,-)}} \right]_{|S} + \left[H_{\mathcal{G}_i}(U_{\mathcal{G}_i})_{|_{F(S,+)}} \right]_{|S} \right) \right\|_{\mathcal{U}^S}^2 \Bigg),
\end{aligned} \tag{5.2}$$

where $\mathcal{H}^S := H^{\frac{1}{2}}(S)$ as in Section 4.1 and the indices $i, j \in \mathfrak{G}$ used in the sums are those of the appropriate fracture groups containing the given trace S.

The constraints for the optimization of $\hat{J}(\hat{U})$ are given by the field equations on each fracture group, expressed in 5.1, with the definitions

$$\begin{aligned}
U_{\mathcal{G}_i}^S &:= \left[\!\left[\frac{\partial H_{\mathcal{G}_i}}{\partial \nu_S^{\mathcal{G}_i}} \right]\!\right] + \alpha H_{\mathcal{G}_i|S}, && S \in \mathcal{S}_{\mathcal{G}}^{\text{ext}}, \mathcal{G}_i \supset S, \\
U_{\mathcal{G}_i,\text{int}}^{S,*} &:= \left[\!\left[\frac{\partial H_{F(S,*)}}{\partial \nu_S^{F(S,*)}} \right]\!\right] + \alpha \left[H_{\mathcal{G}_i|_{F(S,*)}} \right]_{|S}, && S \in \hat{\mathcal{S}}_{\mathcal{G}}^{\text{int}}, \mathcal{G}_i \supset S, * \in \{-,+\},
\end{aligned}$$

where $\alpha > 0$.

5.2 Discrete formulation

Each group of fractures $\mathcal{G}_i$ can be discretized through a conforming mesh, constituted by the set of polygons $\mathcal{T}_{\mathcal{G}_i,\delta} = \mathcal{T}_{\mathcal{G}_i,\delta}^{\text{VEM}} \cup \mathcal{T}_{\mathcal{G}_i,\delta}^{\text{FEM}}$ as done in Section 3.2 for the full domain. The traces involved in the conforming process on $\mathcal{G}_i$ are the ones in the set $\mathcal{S}_{\mathcal{G}_i}^{\text{int}} \setminus \hat{\mathcal{S}}_{\mathcal{G}_i}^{\text{int}}$. The resulting finite dimensional spaces, with order $k = 1$, are

$$\begin{aligned}
V_{\mathcal{G}_i,\delta}^1 = \big\{ v \in V_{\mathcal{G}_i} : & v_{|E_{\text{VEM}}} \in V_1^{\text{VEM}}(E_{\text{VEM}}) \quad \forall E_{\text{VEM}} \in \mathcal{T}_{\mathcal{G}_i,\delta}^{\text{VEM}}, \\
& v_{|E_{\text{FEM}}} \in V_1^{\text{FEM}}(E_{\text{FEM}}) \quad \forall E_{\text{FEM}} \in \mathcal{T}_{\mathcal{G}_i,\delta}^{\text{FEM}} \big\} \\
V_{\mathcal{G}_i,\delta}^{D,1} = \big\{ v \in V_{\mathcal{G}_i}^D : & v_{|E_{\text{VEM}}} \in V_1^{\text{VEM}}(E_{\text{VEM}}) \quad \forall E_{\text{VEM}} \in \mathcal{T}_{\mathcal{G}_i,\delta}^{\text{VEM}}, \\
& v_{|E_{\text{FEM}}} \in V_1^{\text{FEM}}(E_{\text{FEM}}) \quad \forall E_{\text{FEM}} \in \mathcal{T}_{\mathcal{G}_i,\delta}^{\text{FEM}} \big\}.
\end{aligned}$$

For each trace $S \in \mathcal{S}_{\mathcal{G}_i}^{\text{ext}}$, a mesh $\mathcal{T}_{\delta,\mathcal{G}_i}^{S}$ can be considered, together with the associated discrete space $W_{\delta,\mathcal{G}_i}^{S} \subset L^2(S)$, while, for each trace $S \in \hat{\mathcal{S}}_{\mathcal{G}_i}^{\text{int}}$, define the two meshes $\mathcal{T}_{\delta,\mathcal{G}_i}^{S,-}$ and $\mathcal{T}_{\delta,\mathcal{G}_i}^{S,+}$, along with the associated discrete spaces $W_{\delta,\mathcal{G}_i}^{S,-} \subset L^2(S)$ and $W_{\delta,\mathcal{G}_i}^{S,+} \subset L^2(S)$. A similar procedure to that of Section 4.2 can then be followed, where the spaces for the fracture groups fulfill the function of the discrete spaces on single fractures, and some modifications are needed to adapt the method to the discrete spaces for the traces.

Chapter 6

Conclusions

In this work, the problem of the distribution of the hydraulic head of a fluid in a Discrete Fracture Network, modeled as intersecting plane polygons, is considered. Two existing numerical approaches to the computation of the solution are discussed. One is based on a mesh which conforms to the traces and employs a VEM discretization, while the other requires the minimization of a suitable functional constrained by the field equations on fractures, discretized with meshes that do not conform to the traces. Numerical results of first order implementations of the two methods are presented. The numerical tests of the non-conforming optimization approach showed that the condition number of the matrix of the resulting system depends strongly on the length of the mesh segments on the traces, relative to the fractures' mesh size, causing problems for networks with very short traces. The comparison with the conforming VEM approach revealed that the optimization approach results in a linear system with worse conditioning, while achieving a similar level of accuracy. A joint approach is proposed, aimed at excluding short traces from the optimization process and difficult geometries from the conforming meshes, while retaining a structure similar to the one of the optimization approach. Formal results about the joint formulation and numerical testing of the method are not yet discussed.

Bibliography

[1] L Beirão da Veiga et al. "Virtual Element Method for general second-order elliptic problems on polygonal meshes". eng. In: *Mathematical models methods in applied sciences* 26.4 (2016), pp. 729–750. ISSN: 0218-2025.

[2] L. Beirão da Veiga et al. "Basic principles of Virtual Element Methods". eng. In: *Mathematical models methods in applied sciences* 23.1 (2013), pp. 199–214. ISSN: 0218-2025.

[3] L. Beirão da Veiga et al. "The Hitchhiker's Guide to the Virtual Element Method". eng. In: *Mathematical models methods in applied sciences* 24.8 (2014), pp. 1541–1573. ISSN: 0218-2025.

[4] M. F. Benedetto, S. Berrone, and S. Scialò. "A globally conforming method for solving flow in discrete fracture networks using the Virtual Element Method". eng. In: *Finite elements in analysis and design* 109 (2016), pp. 23–36. ISSN: 0168-874X.

[5] M. F. Benedetto et al. "A hybrid mortar virtual element method for discrete fracture network simulations". eng. In: *Journal of computational physics* 306 (2016), pp. 148–166. ISSN: 0021-9991.

[6] S. Berrone, A. Borio, and F. Vicini. "Reliable a posteriori mesh adaptivity in Discrete Fracture Network flow simulations". eng. In: *Computer methods in applied mechanics and engineering* 354 (2019), pp. 904–931. ISSN: 0045-7825.

[7] S. Berrone, S. Pieraccini, and S. Scialo. "A PDE-Constrained Optimization Formulation for Discrete Fracture Network Flows". eng. In: *SIAM journal on scientific computing* 35.2 (2013), B487–B510. ISSN: 1064-8275.

[8] S. Berrone, S. Pieraccini, and S. Scialò. "An optimization approach for large scale simulations of discrete fracture network flows". eng. In: *Journal of computational physics* 256 (2014), pp. 838–853. ISSN: 0021-9991.

[9] S. Berrone and F. Vicini. "A Reduced Basis Method for a PDE-constrained optimization formulation in Discrete Fracture Network flow simulations". eng. In: *Computers mathematics with applications (1987)* 99 (2021), pp. 182–194. ISSN: 0898-1221.

[10] S. Berrone et al. "A Parallel Solver for Large Scale DFN Flow Simulations". eng. In: *SIAM journal on scientific computing* 37.3 (2015), pp. C285–C306. ISSN: 1064-8275.